

# Chiral symmetry breaking and instantons in both quenched and full QCD

U. Sharan and M. Teper

*Theoretical Physics, University of Oxford, 1 Keble Road, Oxford, OX1 3NP, U.K.*

## Abstract

We investigate the contribution that instantons make to the QCD chiral condensate for  $N_f = 0, 1$  and 2 quark flavours. We use a simplified model: the instantons are a (weighted) gas, the fermionic integrations are restricted to the subspace spanned by the would-be zero-modes and only the dimensional and chiral features of the Dirac operator are retained. Previous work along these lines found a power-like divergence of the Dirac spectral density at zero eigenvalue. By changing the various components of the model, we show that a power divergence appears to be a generic feature of instanton mixing for both  $N_f = 0$  and  $N_f \neq 0$ . In the latter case the divergence disappears as  $m \rightarrow 0$  in such a way that  $\langle \bar{\psi}\psi \rangle$  remains finite. We find that the exponent of the power decreases for larger instanton densities, becoming negligible for very dense instanton ‘gases’. We reproduce the expected  $m$ -dependence of the topological susceptibility, we investigate the space-time structure of the eigenfunctions, as a function of the eigenvalue, and we calculate the  $\eta'$  mass. In summary: instantons appear to provide a natural mechanism for the spontaneous breaking of chiral symmetry in QCD, but they typically produce a power-like divergence in the Dirac spectral density. This divergence is non-standard but ‘harmless’ in the case of full QCD, and implies a pathology in the case of quenched QCD.

## I. INTRODUCTION

The spontaneous breaking of chiral symmetry, and the dynamics that drives it, remains a major unsolved problem in QCD. However it has long been recognised [1–3] that instantons provide a potential mechanism for this symmetry breaking. This can be simply motivated using the well-known Banks-Casher formula [4] and the Atiyah-Singer Index theorem [5]. The Banks-Casher formula relates the value of the chiral condensate to the density of modes of the Dirac operator,  $\bar{\nu}(\lambda)$ , at zero eigenvalue:

$$\langle \bar{\psi}\psi \rangle = \pi \bar{\nu}(0), \quad (1)$$

while the Atiyah-Singer Index theorem tells us that the eigenvalue spectrum of the Dirac operator will contain

$$Q[A] = n_- - n_+ \quad (2)$$

exact zero modes, where  $Q[A]$  is the winding number of the gauge field configuration and  $n_{\pm}$  are the number of zero eigenmodes with positive/negative chirality. So if we neglect interactions amongst (anti)instantons we get an exact zero-mode for each topological charge in the gauge field. This contributes a term  $\propto \delta(\lambda)$  to  $\bar{\nu}(\lambda)$ . That is to say, the eigenvalues are clustered about zero. This is in contrast to a purely perturbative approach where, if we neglect interactions, the perturbative vacuum becomes free and the eigenvalue spectrum grows as  $\lambda^3$ . That is to say, the eigenvalues are far from zero. Introducing interactions will shift both these distributions in ways that are not easy to predict once the interactions are strong. Nonetheless it is plausible that if what one wants is a non-zero density of modes near  $\lambda = 0$  then instantons provide a much more promising starting point than the classical vacuum.

An old approach to obtaining chiral symmetry breaking from instantons is as a self-consistent solution to semi-classical gap equations (see, for example, [6]). An alternative approach is to perform a direct calculation of  $\langle \bar{\psi}\psi \rangle$  in some semi-classical approximation

(see, for example, [2,3,7]). Both approaches make drastic approximations, but the latter has the attraction that these can be easily made explicit. In this paper we develop upon the calculations which were briefly summarised in [7]. We now briefly outline our general approach.

To begin, we must make more precise what it might mean for chiral symmetry breaking to be “due to instantons”. First, it is not at all obvious that the topological charge of a typical gauge field must be in a form that resembles an ensemble of instantons. We will, however, assume that it is. That is to say, we assume that it can be decomposed into localised lumps of unit charge,  $Q = \pm 1$ , which can be characterised by the usual instanton collective coordinates. We shall refer to these lumps as ‘instantons’ even though they will normally be far from the minima of the action. There is some evidence from lattice simulations for this assumption (see, for example, [8,9]). A second problem is that even if the topological charge can be decomposed into an ensemble of ‘instantons’, then the correlations between these topological charges will be influenced by other fluctuations in the gauge fields; for example, those that induce confinement. So when we calculate the Dirac spectrum associated with the instantons (see [10] for an example of such a calculation and [11] for a review of related work) this will inevitably contain the influence of other dynamics. Thus, even if we find that we do have chiral symmetry breaking, it will be unclear to what extent it is due to the instantons *per se* and to what extent it is due to this other dynamics. The simplest way to finesse this ambiguity is to ignore all the correlations and see whether an uncorrelated ensemble of instantons will, by itself, drive chiral symmetry breaking. If so, if we can show that the spontaneous breaking of chiral symmetry is a generic consequence of the most general features of an instanton ensemble, then we can plausibly claim that it is indeed ‘due to instantons’.

Since we are interested in the implications of instantons that are generic rather than due to some special details of the approximations used, it makes sense to avoid details altogether, as far as possible, at least as a first step. Such a minimalist approach, that attempts to include only the essentials of the physics, was developed in [7,12] and we shall

use what is almost the same model here. For the pure gauge theory (i.e.  $N_f = 0$  or quenched QCD) we shall take our instantons to have random positions and we give them some fixed size  $\rho$ . The latter embodies the anomalous breaking of scale invariance, while the former encodes the long distance clustering properties of the field theory. We leave the density of instantons as a free parameter and we ignore the other collective coordinates. If we think of a single topological charge, its Dirac spectrum will contain a zero eigenvalue and other, non-zero, modes. The former is independent of how deformed the instanton is; the latter depend on all the details. So if the symmetry breaking is to be a generic feature of the instanton ensemble, it should depend only on the zero modes. We therefore restrict the fermionic path integral in the background of a particular gauge field to the subspace spanned by the zero-modes of the instantons in that gauge field. That is to say, we are investigating whether chiral symmetry breaking is driven by the would-be topological zero modes. While the existence of a zero mode is independent of detail, its functional form is not. Since we do not know what this form is (and there is no reason to think that the classical form is at all relevant) we will try a number of different functional forms and see what, if anything, is insensitive to the particular choice. In a matrix representation of the Dirac operator, the overall structure is determined by the fact that  $Q = \pm 1$  zero modes have opposite chirality and that  $\gamma_5$  anti-commutes with  $i\not{D}$ . We shall assume that this is all that is important and simplify the calculation accordingly. We shall use the same approach for full QCD (i.e.  $N_f \neq 0$ ) except that we weight the instanton ensembles with the appropriate power of the fermionic determinant. This determinant will also be calculated in the basis of would-be zero-modes as described above.

We remark that the above may be thought of as a ‘bottom-up’ approach to this whole question. There is an alternative approach that one may think of as ‘top-down’. Here one uses random matrix theory (for recent reviews see [13]) identifying the appropriate universality class on the basis of the symmetries in the problem, and then making corresponding predictions for the fermionic physics. To what extent the two approaches are in agreement, even for quantities for which they both make predictions, is not clear to us, but this is a

question that needs to be addressed.

The conclusion of [7,12] was not only that instantons generically produce a non-zero chiral condensate, but that in quenched QCD this condensate diverges as  $m \rightarrow 0$ . This divergence is a reflection of a corresponding power-like divergence,

$$\bar{\nu}(\lambda) = a + b/\lambda^d, \tag{3}$$

as  $\lambda \rightarrow 0$ , in the spectral density. The value of the exponent was found [7,12] to be  $d \simeq 1/2$ . If this is indeed the case, then it suggests a striking pathology in quenched QCD. An essential first step in assessing this result is to determine how robust it is against changes in the assumptions employed. In particular, the zero-modes were modeled, in [7,12], by simple hard-sphere wave-functions (and the wavefunction overlaps were generally calculated using only the space-time points at which the topological charges were located). In the present paper we shall compare calculations with several different functional forms (and we shall use the full overlap functions). We shall also perform a detailed study of finite-volume effects and of how things depend on the instanton density or ‘packing fraction’  $f$ . The latter has a natural definition for ‘hard sphere’ wavefunctions:

$$f \equiv \frac{\bar{N} \bar{V}_I}{V} \tag{4}$$

where  $\bar{N}$  is the mean number of topological objects in the gas,  $\bar{V}_I$  is the mean volume of such an object and  $V$  is the volume of space-time. (Recall that the volume of a 4-sphere of radius  $\rho$  is  $V_I = \pi^2 \rho^4/2$ .) What is the corresponding definition of  $f$  for other wavefunctions is not immediately obvious and is one of the questions we shall address below. Our calculations will lead us to a somewhat more nuanced conclusion than that drawn in [7]. In particular we find that while a divergence is indeed a characteristic product of the mixing of the would-be zero-modes, the value of the exponent depends quite strongly on the instanton density, becoming negligible for large packing fractions.

In full QCD there should be no such pathology, and so it is of interest to ask what happens to this small- $\lambda$  divergence as we make  $N_f \neq 0$ . We find that the divergence is

still there but that its coefficient  $\rightarrow 0$  as the fermion mass  $\rightarrow 0$  in (apparently) such a way that the chiral condensate has the conventional smooth chiral limit. Thus the divergence is ‘harmless’ although the Dirac spectrum is unconventional and the usual Banks-Casher [4] relation, given in equation 1, need no longer be valid.

In the next section we provide a brief discussion of instantons and chiral symmetry breaking which will also serve to introduce our notation. We then introduce our minimalist model for an ensemble of instantons, their associated zero modes and our matrix representation for the Dirac operator. We point to some calculational difficulties and how we deal with these by the choice of an appropriate space-time manifold. We then turn to the results of our calculations for quenched QCD. Our main result is that the Dirac spectrum diverges at small eigenvalues. How this result depends on details, both unphysical – such as the functions chosen for the zero-modes and the space-time manifold in which they exist – and physical – such as the instanton density and the physical volume – is investigated in detail. We also investigate whether the eigenfunction of the Dirac operator changes character as the corresponding eigenvalue decreases. We find that indeed it does: as  $\lambda \rightarrow 0$  the eigenfunction becomes much more non-local. Having acquired some confidence that the qualitative features of our calculations are independent of the specific model assumptions, we then proceed to the (computationally) more difficult case of full QCD. Here we ask whether instantons spontaneously break chiral symmetry, what happens to the  $\lambda \rightarrow 0$  divergence in the Dirac spectral density, and whether our model can correctly reproduce the  $m$ -dependence of the topological susceptibility that is predicted by the anomalous Ward identities. We also calculate the  $\eta'$  mass and confirm that it is not a Goldstone boson.

Some of our early results were summarised in [14]. A calculation of the Dirac spectrum using the cooled instanton ensembles obtained in the SU(3) lattice gauge theory calculation of [8] is to be found in [10]. Although the results differ, in the fine detail, from what one obtains with a randomly placed ensemble of instantons, the main features of spontaneous symmetry breaking and a divergent quenched chiral condensate appear to be present.

## II. CHIRAL SYMMETRY BREAKING AND TOPOLOGY

The usual order parameter for chiral symmetry (breaking) is the chiral condensate in the limit of infinite volume and zero mass:  $\langle \bar{\psi}\psi \rangle = \lim_{m \rightarrow 0} \lim_{V \rightarrow \infty} \langle \bar{\psi}\psi \rangle_{m,V}$ . We can express  $\langle \bar{\psi}\psi \rangle_{m,V}$  in terms of the normalised Dirac spectral density,  $\bar{\nu}(\lambda, m)$ , as

$$\langle \bar{\psi}\psi \rangle_{m,V} = \frac{\bar{N}_Z}{mV} + \int_0^\infty \frac{2m\bar{\nu}(\lambda, m)}{\lambda^2 + m^2} d\lambda. \quad (5)$$

Here we have chosen to separate from  $\bar{\nu}$  the  $\delta$ -function contribution of the exact zero modes, whose mean number is  $\bar{N}_Z = |\overline{Q}| \propto \sqrt{V}$ . In the thermodynamic limit this zero-mode contribution will clearly disappear. Thus one might expect that at finite- $V$  the eigenvalue spectrum restricted to  $Q = 0$  field configurations will have smaller finite- $V$  corrections than if we allow  $Q$  to vary. (As long as the total number of topological charges is  $N \gg 1$ , so that we would have had  $\langle Q^2 \rangle \gg 1$  if we had allowed  $Q$  to vary, this should not represent an unphysical bias on the calculation.) In this expectation (to be verified later on) most of the calculations in this paper will be for fields with  $Q = 0$ .

Note that if we work in a finite volume, then we would normally choose it to be at least large enough to accommodate the lightest particle in the theory, the Goldstone pion, i.e.  $V^{\frac{1}{4}} \sim 1/m_\pi$ . If we insert  $m_\pi^2 f_\pi^2 = m \langle \bar{\psi}\psi \rangle$  and crudely estimate  $\bar{N}_Z \simeq \sqrt{\langle Q^2 \rangle} = \sqrt{\chi_t V}$ , where  $\chi_t$  is the topological susceptibility, then we find that the zero-mode contribution in equation 5 is

$$\frac{\bar{N}_Z}{mV} \sim \frac{\chi_t^{\frac{1}{2}}}{f_\pi^2} \langle \bar{\psi}\psi \rangle \sim 4 \langle \bar{\psi}\psi \rangle \quad (6)$$

where we have used the standard values,  $\chi_t \sim (180 \text{ MeV})^4$  and  $f_\pi \sim 93 \text{ MeV}$ . This demonstrates that the finite-volume correction to the quenched QCD chiral condensate from the exact zero-modes can be large even if one uses space-time volumes that might appear to be adequate.

In full QCD the above calculation will differ in that the topological susceptibility will vary with the quark mass:  $\chi_t \simeq m \langle \bar{\psi}\psi \rangle / n_f^2$  if we have spontaneous chiral symmetry breaking. Inserting this into equation 6 we find that the zero-mode contribution

$$\frac{\overline{N}_Z}{mV} \sim \frac{\sqrt{\chi_t V}}{mV} \sim \frac{1}{(mV)^{\frac{1}{2}}} \frac{\langle \overline{\psi}\psi \rangle^{\frac{1}{2}}}{N_f} \propto m^{\frac{1}{2}} \quad (7)$$

vanishes when we take the chiral limit while maintaining  $V$  large enough to accommodate the Goldstone pion. Note that the case of a single flavour,  $N_f = 1$ , is special. Now there will be no Goldstone pion because the  $U_A(1)$  symmetry is anomalous: the would-be pion is a massive  $\eta'$ . So there is a finite mass-gap in the theory as  $m \rightarrow 0$ . In such a situation one would normally expect that a fixed finite volume, with  $V^{\frac{1}{4}} > 1/m_{\eta'}$ , would be large enough. However we note that this would lead to a  $\propto 1/\sqrt{m}$  divergence in the chiral condensate.

One can ask what happens to the zero-mode contribution if one chooses to take the chiral limit in a fixed volume. In that case we expect symmetry restoration for sufficiently small  $m$ , and for smaller masses we may expect  $\chi_t \propto m^{N_f}$ . Thus for  $N_f \geq 2$  there will be no real  $m \rightarrow 0$  divergence in  $\langle \overline{\psi}\psi \rangle_{m,V}$  at fixed  $V$ .

The above finite volume corrections, due to the  $|Q|$  exact zero modes, induce a trivial divergence in the  $N_f = 0$  chiral condensate if we take the  $m \rightarrow 0$  chiral limit at fixed volume. As remarked earlier, we shall evade this divergence by usually working with  $Q = 0$  field configurations. However, as described in the introduction, there is evidence [7,12,14] for a much less trivial divergence; one which survives the thermodynamic limit and which appears as a divergence in the spectral density of the form in equation 3. One of the main aims of this paper is to determine whether this divergence is really there, in both quenched and full QCD, or whether it is an artefact of the approximations used in the calculations of [7,12,14].

There is a simple argument [7,12], briefly described in [7], that provides an apparently natural explanation for such a divergence. It goes as follows.

In a finite volume  $V$  one expects to lose spontaneous symmetry breaking once the explicit symmetry breaking term is small enough i.e. once  $mV$  becomes small. That is to say, we expect a suppression in the finite volume spectral density for  $|\lambda| < O(1/V)$ . Let us assume, for simplicity, that the only finite- $V$  correction affecting the spectral density of the non-zero modes consists of a cut-off for  $|\lambda| < c/V$ . Then the only other finite- $V$  correction



concerns the exact zero-modes. If we increase the volume from  $V$  to  $V'$  then their number increases from  $n_z \sim \sqrt{\langle Q^2 \rangle} \sim \sqrt{\chi_t V}$  to  $\sim \sqrt{\chi_t V'}$ . Therefore, as a fraction of the total number of modes, their number will decrease from  $\sim \sqrt{\chi_t/V}$  to  $\sim \sqrt{\chi_t/V'}$ . The integrated spectral density (including the zero modes) does not change with volume so these two finite- $V$  corrections must match:

$$\int_{\frac{c}{V'}}^{\frac{c}{V}} \bar{\nu}(\lambda) d\lambda = \sqrt{\frac{\chi_t}{V}} - \sqrt{\frac{\chi_t}{V'}}. \quad (8)$$

where  $\bar{\nu}(\lambda)$  is the spectral density for  $V = \infty$ . It is easy to see that this relation implies that

$$\bar{\nu}(\lambda) \stackrel{\lambda \rightarrow 0}{\propto} \lambda^{-\frac{1}{2}} \quad (9)$$

and hence that  $\langle \bar{\psi} \psi \rangle \propto m^{-\frac{1}{2}}$  in the thermodynamic, chiral limit.

The important assumption in this argument is that as we increase the volume, the fractional decrease in the exact zero-modes is matched by an increase amongst the very smallest of the non-zero modes. We shall refer to this as the ‘‘eigenvalue replacement hypothesis’’ and shall investigate it in more detail later on in this paper. For now we simply point out that intuitively it is not unreasonable. In a volume  $V$  we expect on the average  $c_0 \sqrt{V}$  exact zero modes. Now consider this volume split into two equal halves. Considered in isolation each half-volume would possess  $\sim c_0 \sqrt{V/2}$  exact zero-modes. So in joining these two half-volumes together we have decreased the total number of zero modes from  $\sim 2 \times c_0 \sqrt{V/2} = c_0 \sqrt{2V}$  to  $c_0 \sqrt{V}$ . That means some of the original zero-modes have mixed and split from zero. But if  $V$  is sufficiently large, one would expect the zero modes in the two halves to be mostly far from each other so that the overlap will be very small, and the eigenvalues will be split very little from zero. This very qualitative argument should really be formulated using a number of subvolumes for which one can use statistical arguments. But it suffices to give some motivation for what we have called the eigenvalue replacement hypothesis.

The above argument would seem to be equally applicable to full QCD, with one modification: now  $\chi_t \propto m$  (as long as chiral symmetry is spontaneously broken). Inserting this into equation 8 we find

$$\bar{\nu}(\lambda) \stackrel{\lambda \rightarrow 0}{\propto} \left(\frac{m}{\lambda}\right)^{\frac{1}{2}}. \quad (10)$$

While this is an unconventional form for the spectral density, it does not create any divergence in the chiral condensate:

$$\begin{aligned} \langle \bar{\psi}\psi \rangle &= \lim_{m \rightarrow 0} \lim_{V \rightarrow \infty} \langle \bar{\psi}\psi \rangle_{m,V} \\ &= \lim_{m \rightarrow 0} \int_0^\infty \frac{2m\bar{\nu}(\lambda, m)}{\lambda^2 + m^2} d\lambda \\ &= \lim_{m \rightarrow 0} \int_0^\infty \frac{2m\{a + b(\frac{m}{\lambda})^{\frac{1}{2}}\}}{\lambda^2 + m^2} d\lambda \\ &= \int_0^\infty \frac{2\{a + \frac{b}{y^{\frac{1}{2}}}\}}{y^2 + 1} dy \\ &= \pi a + 2b \int_0^\infty \frac{dy}{y^{\frac{1}{2}}(y^2 + 1)}. \end{aligned} \quad (11)$$

Here we have used a spectrum  $\bar{\nu}(\lambda) = a + b(m/\lambda)^{\frac{1}{2}}$  and have performed a change of variable to  $y = \lambda/m$ . We see that the result for  $\langle \bar{\psi}\psi \rangle$  is finite. However the naive application of the Banks-Casher formula, which would have produced the result  $a\pi$ , breaks down. So, although a spectral density of this kind does not immediately lead to any pathological physics, it is clear that it might undermine any argument which relies on the  $\lambda \rightarrow 0$  and  $m \rightarrow 0$  limits commuting with each other.

The form we conjecture in equation 10 can also be made plausible as follows. Since a mode of  $i\mathcal{D}$  will not be (individually) suppressed by the  $(\det i\mathcal{D})^{N_f} = \prod (\lambda_i^2 + m^2)^{N_f}$  weighting if  $\lambda \ll m$ , we might expect that the spectral density for full QCD will have the same form as in quenched QCD for  $\lambda \ll m$ . If the quenched spectrum behaves as  $1/\lambda^{\frac{1}{2}}$  as  $\lambda \rightarrow 0$  then the spectrum of full QCD should have the form  $\bar{\nu}(\lambda, m) = (\mu/\lambda)^{\frac{1}{2}}$  for  $\lambda \ll m$  where  $\mu$  will have dimensions of mass, just on dimensional grounds. The theory has two dimensionful parameters: the quark mass  $m$  and the pure gauge scale  $\Lambda_{QCD}$ . Since the term  $(\mu/\lambda)^{\frac{1}{2}}$  should only become important (compared to the constant term say) for  $\lambda \ll m$ , it must be that  $\mu \propto m$ . That is to say, the form in equation 10.

If we use the argument in the previous paragraph, then we can reverse our earlier argument in order to show that in QCD we should have  $\langle Q^2 \rangle \propto mV$ . This is of interest because it

is actually hard to find a simple explicit argument that gives this result. (The usual derivation using anomalous Ward identities may be simple but is hardly explicit.) For example, if we take the dilute gas limit then each topological charge has its separate fermionic weighting  $\propto (\det i\mathcal{D}[A_I])^{N_f} \propto m^{N_f}$  that accompanies the factor of  $V$  (the charge can be located anywhere in the space-time volume). One immediately concludes that  $\langle Q^2 \rangle \propto m^{N_f} V$ . Suppose instead we try the opposite extreme, where the only important effect of the fermionic weighting is that the gauge field acquires a factor  $\propto m^{N_f|Q|}$ . If we had just a pure gauge weighting, then we would have  $\langle Q^2 \rangle \propto V$ , and for  $Q^2 \ll V$  the weighting will be almost independent of  $Q$ . For such  $Q$  the only non-trivial weighting is our assumed fermionic weighting  $\propto m^{N_f|Q|} = \exp\{-N_f|Q| \ln(1/m)\}$ . It is easy to see that this implies  $\langle Q^2 \rangle \propto m^{N_f}$ . (Now we do not even have the correct factor of  $V$ .) It is clear that the real situation is much more subtle. When we have chiral symmetry breaking the spectral density remains finite all the way down to  $\lambda = 0$ . So the  $|Q|$  exact zero-modes may have been traded for modes that were arbitrarily close to zero. It is this effect that presumably reduces the naive  $\langle Q^2 \rangle \propto m^{N_f} V$  dependence (which is correct when we have chiral symmetry restoration and no non-trivial density of modes arbitrarily close to zero) to the weaker  $\langle Q^2 \rangle \propto mV$  dependence. It will be interesting to see whether we can reproduce this subtle trade-off within the simple model that we shall be using in this paper.

### III. THE MODEL

In this section we describe how we are going to calculate the contribution of instantons to the Dirac spectral density. This requires making a number of radical simplifications. Although we shall try to give each of these simplifications some motivation, it is important to perform some check that the final conclusions are robust against changes in the assumptions being made.

We shall first describe the general framework of our calculation. (We refer the reader to [10] for a detailed discussion of some aspects of the model.) We shall then describe the

various zero-mode wave functions that we use in our calculations. Comparing the results of these calculations will provide a check of the robustness of our scheme.

### A. The general strategy

We are interested in determining what are the generic physical effects of instantons. Suppose we have a gauge field which contains  $n_I$  instantons and  $n_{\bar{I}}$  anti-instantons. Suppose that the fields of the instantons and anti-instantons, if in isolation, would be  $A_i^+$  and  $A_i^-$  respectively. Using a linear addition approximation one can write a field

$$A = \sum_i^{n_{\bar{I}}} A_i^+ + \sum_j^{n_I} A_j^- \quad (12)$$

that represents the instanton content of the original gauge field. (We suppose that each individual instanton field is in a suitable singular gauge so as to be as local as possible.) One could do this for a realistic ensemble of (lattice) gauge fields, as was done in [10]. However in that case there will be correlations amongst the instantons that are partly determined by other, non-topological fluctuations and if we are interested in the generic properties of instantons *per se* then we do not want to include these. So the fields we shall consider will be those due to a randomly positioned ensemble of instantons. Such an ensemble clearly possesses the long-distance clustering properties of the field theory. We shall give the instantons a specific size; this embodies the anomalous scale-breaking in the theory. The instanton size sets the length scale of the theory and the volume of space-time can be expressed in those units. Varying the average distance between instantons amounts to varying the density, or packing fraction, as defined earlier. A slightly more elaborate approach would be to give the instantons a distribution of sizes; in particular for small sizes the distribution is calculable in perturbation theory. For the results of such an approach we refer the reader to [10].

The above is plausible for quenched QCD, but breaks down for full QCD where the correlations between topological charges will become of increasingly long range as  $m \rightarrow 0$ .

This can be incorporated by weighting the instanton ensemble by a factor  $\propto (\det i\mathcal{D})^{N_f}$ . This will be described in detail later on in the paper.

There are a total of  $N[A] = n_{\bar{I}} + n_I$  objects in our gauge field  $A$  (in the volume  $V$ ), and the winding number of  $A$  is  $Q[A] = n_I - n_{\bar{I}}$ . We know via the Atiyah-Singer Index Theorem [5] that the Dirac operator in this background  $i\mathcal{D}[A]$  will have at least  $Q[A]$  exact zero eigenvalues. If the objects in the superposition were non-interacting then each would have a corresponding zero eigenvalue,

$$i\mathcal{D}[A_i^\pm]\psi_{i0}^\pm = 0, \quad (13)$$

again due to the Atiyah-Singer Index Theorem. We see from equation 13 that these zero modes are modes of definite chirality, in fact  $\gamma^5|\psi_{i0}^\pm\rangle = \pm|\psi_{i0}^\pm\rangle$ . Interactions between the objects however, lead to a reduction of exact zero modes from  $N[A]$  to only  $Q[A]$ . The remaining  $N[A] - Q[A]$  modes have split symmetrically about zero [3,2,10]. We shall frequently refer to these modes as the “would-be zero modes”. The model, which is by no means new, is based around the idea of constructing an explicit matrix representation of the Dirac operator, using only the zero mode wavefunctions  $\{|\psi_{i0}^+\rangle, |\psi_{j0}^-\rangle\}$  as a basis. Of course, the claim is not that these zero mode wavefunctions in isolation form a basis (they certainly do not span), the claim is that by constructing the Dirac operator on this subspace we can understand that part of the Dirac spectrum which arises from instanton interactions. Furthermore as these are the eigenvalues which generate a spectral density around zero, we may be able to comment upon the idea of instantons as the source of chiral symmetry breaking in QCD. We drop the subscript zeroes on the would be zero mode wavefunctions from now on, as these are the only wavefunctions which we shall consider. It is easy to see that:

$$\begin{aligned} \langle\psi_i^+|i\mathcal{D}[A]|\psi_j^+\rangle &= 0 \\ \langle\psi_i^-|i\mathcal{D}[A]|\psi_j^-\rangle &= 0 \\ \langle\psi_i^+|i\mathcal{D}[A]|\psi_j^-\rangle &\doteq V_{ij}. \end{aligned} \quad (14)$$

The first two identities follow from  $\{i\mathcal{D}, \gamma^5\} = 0$  and the definite chirality of the zero mode

wavefunctions. The function  $V_{ij}$  can in principle depend upon the size, position and relative colour orientation of all the objects in the field. We shall ignore the colour orientation of the objects for simplicity. And we shall assume that  $V_{ij}$  depends only on the objects  $i$  and  $j$ . This is an approximation that becomes increasingly hard to justify as the instantons become denser. See [10] for a more detailed discussion. We also note that:

$$\begin{aligned}
\langle \psi_i^+ | \psi_j^+ \rangle &= U(x_i^+, \rho_i^+, x_j^+, \rho_j^+) \\
\langle \psi_i^- | \psi_j^- \rangle &= U(x_i^-, \rho_i^-, x_j^-, \rho_j^-) \\
\langle \psi_i^\pm | \psi_j^\mp \rangle &= 0,
\end{aligned} \tag{15}$$

simply from the chiral properties of the zero mode wavefunctions. The function  $U$  will depend upon the size, position and relative colour orientation (which we ignore) of the objects. We now use equation 15 to construct an orthonormal set of vectors  $\{|\tilde{\psi}_i^+\rangle, |\tilde{\psi}_j^-\rangle\}$  using Gram-Schmidt orthonormalization:

$$\begin{aligned}
|\psi_j^+\rangle &= R_{ij} |\tilde{\psi}_i^+\rangle \quad 1 \leq i \leq j \leq n_T \\
|\psi_j^-\rangle &= S_{ij} |\tilde{\psi}_i^-\rangle \quad 1 \leq i \leq j \leq n_I.
\end{aligned} \tag{16}$$

A representation of the Dirac operator (in this restricted subspace) is given by:

$$i\mathcal{D} \doteq \tilde{D} = \left( \begin{array}{cc} \overbrace{\langle \tilde{\psi}_i^+ | i\mathcal{D} | \tilde{\psi}_j^+ \rangle = 0}^{n_T} & \overbrace{\langle \tilde{\psi}_i^+ | i\mathcal{D} | \tilde{\psi}_j^- \rangle = \tilde{V}_{ij}}^{n_I} \\ \overbrace{\langle \tilde{\psi}_i^- | i\mathcal{D} | \tilde{\psi}_j^+ \rangle = \tilde{V}_{ij}^\dagger}^{n_T} & \overbrace{\langle \tilde{\psi}_i^- | i\mathcal{D} | \tilde{\psi}_j^- \rangle = 0}^{n_I} \end{array} \right) \left. \begin{array}{l} \} n_T \\ \} n_I \end{array} \right) \tag{17}$$

where

$$\tilde{V} = (R^{-1})^\dagger V S^{-1} \tag{18}$$

We can therefore construct this matrix representation for any given configuration of instantons providing we have been given the functions  $U(x_i^\pm, \rho_i^\pm, x_j^\pm, \rho_j^\pm)$  and  $V(x_i^\pm, \rho_i^\pm, x_j^\mp, \rho_j^\mp)$ . Once we have the matrix it is a simple matter to calculate its eigenvalues and build up a spectral density using an ensemble of configurations.

The function  $U$  will depend on the functional form of the would-be zero modes. What this form is, in a realistic gauge field, is not known, apart from the fact that one expects it to be localised around the centre of the instanton and to have an extent that is related to the size of the instanton. (We remark that there is no particular reason to favour the known semi-classical zero-mode solution.) We assume that apart from the chirality, the spinorial degrees of freedom are inessential. We will therefore use wave-functions that are simple real valued functions of position, with an index,  $+$  or  $-$ , to label the chirality. We shall use several simple trial functional forms, as described in detail below. Only those features of the resulting Dirac spectrum that are independent of the wave-function form used, can be considered to be generic features of instanton physics.

The function  $V$  depends not only on the form of the would-be zero modes but also on what we choose for  $i\mathcal{D}$ . If all the other fields have a negligible presence in the region where  $\psi_l^-(x)$  and  $\psi_k^+(x)$  are non-zero, then we can write

$$\begin{aligned}
V_{kl} &= \langle \psi_k^+ | i\mathcal{D}[A] | \psi_l^- \rangle \\
&\approx \langle \psi_k^+ | i\mathcal{D}[\sum_i A_i^+ + \sum_j A_j^-] | \psi_l^- \rangle \\
&\approx \langle \psi_k^+ | i\mathcal{D}[A_k^+ + A_l^-] | \psi_l^- \rangle \\
&= \langle \psi_k^+ | i\mathcal{D}[A_k^+] + i\mathcal{D}[A_l^-] - i\mathcal{D} | \psi_l^- \rangle \\
&= \langle \psi_k^+ | -i\mathcal{D} | \psi_l^- \rangle
\end{aligned} \tag{19}$$

Here the first approximation is a consequence of the linear addition ansatz as stated previously. The second approximation holds if the objects are well separated from one another, however it does not hold in general (especially for the high density gases to which we sometimes apply our model). It is however necessary if we are to progress beyond the ‘‘dilute’’ gas approximation using a model such as ours. The last two equalities hold due to the fact that the states are zero-modes:  $i\mathcal{D}[A_l^\pm]|\psi_l^\pm\rangle = 0$ . Of course in any realistic situation this matrix element will depend in a complicated way on all the other fields. We can only hope to elucidate those properties that are independent of this unknown dependence. In that case

it makes sense to begin by simplifying this operator as radically as possible; that is to say, we retain only its dimensionality and its chiral properties. So, apart from anticommuting with  $\gamma_5$ , we assume that the Dirac operator acts like a unit operator multiplied by a scale factor  $1/\rho$  where  $\rho$  is a characteristic length scale of the matrix element under consideration. We choose to use  $\rho \equiv \sqrt{\rho_i \rho_j}$  for the matrix element  $V_{ij}$  (so ignoring the scale provided by the distance between the instanton and anti-instanton):

$$V_{ij} \simeq \frac{1}{\sqrt{\rho_i \rho_j}} \int d^4x \psi_j^-(x) \psi_i^+(x) \quad (20)$$

While extreme, we note that this choice has the correct qualitative behaviour in the dilute gas limit: all the eigenvalues go to zero. Of course in this limit the splitting from zero will depend on the detailed form of the tails of the zero-modes. In the opposite limit, where the density becomes large, our basis of zero-modes eventually becomes complete and it is easy to see that our matrix  $V$  will tend to the unit matrix divided by the size  $\rho$  (assuming the size is fixed). Note that if we had tried to do better than equation 20 and had replaced  $i\mathcal{D}[A]$  by  $i\mathcal{D}$ , then the eigenvalue spectrum of  $V$  would tend to that of the free fermion spectrum as the basis becomes complete. This is of course no reason to panic; this limit is clearly unphysical and in any case all our simplifying assumptions will have certainly broken down by then. However it explains why in our calculations, when we vary the density, we find that at high densities our eigenvalue spectra appear to tend towards  $\propto \delta(\lambda - 1/\rho)$ .

To obtain some idea of the errors induced by this simplification, we shall in at least one case below, use a more realistic version of the Dirac operator.

## B. Zero-mode wave functions

Since our calculations are in part numerical, we can only deal with a finite number of instantons. That is to say, we will work in a finite space-time volume. Of course, we are primarily interested in the  $V \rightarrow \infty$  limit and so we want the finite volume corrections to be as small as possible. This can usually be achieved by working in a periodic box,  $\mathbb{T}^4$ . The



wave-functions also then need to be periodic. The calculation of the overlaps will usually be too complicated to be performed analytically and will then need to be performed numerically. This calculation has to be performed to a very high precision, otherwise our orthogonalisation procedure will occasionally break down. With a large number of topological charges, accurate numerical calculations of overlaps can become prohibitively expensive. This means that in practice the wavefunctions that we can use on a (hyper)torus are quite limited.

An alternative to working on  $\mathbb{T}^4$  is to calculate overlaps within  $\mathbb{R}^4$  while locating the centres of the instantons within a finite space-time volume  $V$ . As  $V \rightarrow \infty$  one will obtain the same spectrum as one obtains by taking the volume of  $\mathbb{T}^4$  to infinity. The drawback is that finite volume corrections are likely to be much larger than for a torus. The obvious advantage is that it is possible to do efficient calculations with a much larger range of trial wavefunctions. For the sake of brevity we shall refer to such calculations as being performed “in  $\mathbb{R}^4$ ”.

We now list the various wave functions we shall be using in this paper.

### 1. Hard sphere

The hard sphere wavefunction is defined by:

$$\begin{aligned} \langle x | \psi_{Hj}^\pm \rangle &= 1 & |x - x_j^\pm| \leq \rho_j^\pm \\ &= 0 & \text{otherwise,} \end{aligned} \tag{21}$$

where  $\rho_j^\pm$  is the measure of its size and  $x_j^\pm$  is its centre. This is the simplest wavefunction we use. In  $\mathbb{R}^4$  the overlap is simply given by the volume of intersection between two solid balls in four dimensional space and this is easy to calculate analytically.

If we are in  $\mathbb{T}^4$  and if  $\rho_j \leq l/2$ , where  $l$  is the length of the torus, then the periodic copies of the hard sphere do not overlap with each other. This greatly simplifies the calculation of the overlap matrix element  $U_{ij}$ ; we just calculate the overlap between the  $j$ 'th object and the  $i$ 'th object as well as with all the nearest periodic copies of the  $i$ 'th object, and each of

these calculations can be performed analytically as though in  $\mathbb{R}^4$ . If  $\rho_j \leq l/4$  things become even simpler since the periodic copies then make no contribution.

Thus the calculations with  $\psi_H(x)$  can be performed efficiently in both  $\mathbb{T}^4$  and  $\mathbb{R}^4$ . Hence it is the wavefunction that was used in the calculations of [7] and in [10]. It has some obvious drawbacks. In even a moderately dilute gas there will be some instantons which have no overlap with any anti-instantons and these will produce ‘accidental’ exact zero-modes. Moreover, one can easily show that in a dilute gas there is a trivial  $1/\lambda^{0.6}$  divergence in the eigenvalue spectrum as  $\lambda \rightarrow 0$ , that arises from the two-body eigenvalue splitting that results from isolated (anti)instanton pairs whose overlap tends to 0. Since a divergence as  $\lambda \rightarrow 0$  is one of the main issues in this paper, we will need to perform careful checks to show that it does not have this trivial origin.

## 2. Gaussian

Gaussian wavefunctions in  $\mathbb{R}^4$  have tails that stretch to infinity and their overlaps can be calculated analytically. The Gaussian wavefunction is given by:

$$\langle x | \psi_{G_j}^\pm \rangle = \frac{1}{\sqrt{2\pi}\sigma_j^\pm} \exp\left(\frac{(x - x_j^\pm)^2}{2\sigma_j^{\pm 2}}\right). \quad (22)$$

where  $x_j^\pm$  is the centre and  $\sigma_j^\pm$  is a measure of its size.

If one wishes to work in  $\mathbb{T}^4$  then this wave-function must be made periodic in some way. We shall choose to do so as follows. First consider the following Gaussian function in  $\mathbb{R}^4$ :

$$G(x; x_j^\pm, \sigma_j^\pm, n) = \frac{1}{\sqrt{2\pi}\sigma_j^\pm} \exp\left(\frac{(x - x_j^\pm - n.l)^2}{2\sigma_j^{\pm 2}}\right), \quad (23)$$

where  $x_j^\pm$  lies in the volume  $V = l^4$  and  $n \in \mathbb{Z}^4$ . Then the following provides a periodic wave-function:

$$\langle x | \psi_{G_j}^\pm \rangle = N \sum_{n \in \mathbb{Z}^4} G(x; x_j^\pm, \sigma_j^\pm, n), \quad (24)$$

where  $N$  is a suitable normalization constant. This is clearly a smooth function on  $\mathbb{T}^4$ , since we have simply added all its periodic copies to our original Gaussian. The overlap of two such

wave-functions over  $\mathbb{T}^4$  is simply the overlap over  $\mathbb{R}^4$  divided by the number of  $\mathbb{T}^4$  subvolumes contained in  $\mathbb{R}^4$ . Each such overlap is a sum of terms each of which consists of the overlap between two simple Gaussians defined on  $\mathbb{R}^4$ . This can be calculated analytically. Hence our reason for choosing this particular periodic extension of the Gaussian wavefunction.

Of course the above procedure involves infinite sums. In practice, however, a Gaussian falls off sufficiently fast with distance that we can often ignore all but the nearest periodic copies, while maintaining a very good precision. When this is so the Gaussian calculation on  $\mathbb{T}^4$  is only about  $3^4$  times slower than the hard sphere calculation. Thus while our largest scale calculations on the torus will be with  $\psi_H$ , we shall be able to perform realistic comparisons with  $\psi_{\tilde{G}}$  when required.

### 3. Classical

The classical zero-mode wave-function in  $\mathbb{R}^4$  is defined by:

$$\langle x|\psi_{Cj}^\pm\rangle = \frac{\sqrt{2}}{\pi} \frac{\omega_j^\pm}{(\omega_j^{\pm 2} + (x - x_j^\pm)^2)^{\frac{3}{2}}}, \quad (25)$$

where  $\omega_j^\pm$  is a size parameter and  $x_j^\pm$  denotes the centre of the object. In the semiclassical limit it would be the correct wavefunction to use, but there is no reason to think that it plays a special role in the full quantum vacuum. It has a slow fall-off with distance and for this reason we do not use it on  $\mathbb{T}^4$ . (The natural way to proceed on  $\mathbb{T}^4$  would be to determine the approximate functional form of the zero-mode numerically and to work with that.)

The overlap calculation is less trivial in this case than for the hard sphere and Gaussian wavefunctions. Using the standard method of Feynman parameters yields the following integral solution:

$$\langle \psi_{Ci}|\psi_{Cj}\rangle = \frac{8}{\pi} \frac{\omega_i}{\omega_j} \int_0^1 dq \frac{\sqrt{q(1-q)}}{1 + q\left(\frac{s^2}{\omega_j^2} + \frac{\omega_i^2}{\omega_j^2}\right) - q^2 \frac{s^2}{\omega_j^2}}. \quad (26)$$

where  $s^2 = (x_i - x_j)^2$ . The lack of a closed form expression for this overlaps makes the calculation far slower than when we use the hard sphere (or even the Gaussian) wavefunction. One

can indeed evaluate this integral in terms of the hypergeometric function of two variables, but the quickest way of evaluating this function is to calculate the above one-dimensional integral numerically.

In the case of this wave-function we shall also perform some calculations that approximate the covariant derivative by the partial derivative, i.e.  $V_{kl} \simeq \langle \psi_k^+ | -i \not{\partial} | \psi_l^- \rangle$ , rather than by the identity, as in equation 20. There are several parameterizations of this matrix element for classical zero mode wavefunctions [3,15], and we shall use the parameterization:

$$\langle \psi_k^+ | -i \not{\partial} | \psi_l^- \rangle \approx \frac{16R}{\rho_k^+ \rho_l^- (2 + R^2/\rho_k^+ \rho_l^-)^2} \quad (27)$$

where  $R = |x_k^+ - x_l^-|$  [3]. We shall label these calculations as “type II classical”. This will provide a non-trivial test of the robustness of our results against the extreme approximation we have made for the covariant derivative.

## IV. QUENCHED QCD ( $N_F=0$ )

### A. Robustness

The most striking result of the early work [7,12] with (essentially) the above model was that the mixing between the would-be instanton zero-modes produced a power-like divergence in the Dirac spectral density as  $\lambda \rightarrow 0$ . The degree of divergence that was found,  $d \simeq 0.5$  in equation 3, fitted in well with the simple theoretical argument given in Section 2. The calculations were, however, only performed with the hard-sphere wave-function,  $\psi_H$ , and for a limited range of volumes and packing fractions. Clearly one needs to test the robustness of this divergence against varying the details of the calculation and this is what we aim to do in this section.

The first question we address is: how large are finite volume corrections when we use the hard-sphere wavefunction on  $\mathbb{T}^4$ ? This is the wavefunction, see equation 21, that was used in [7]. Before presenting our results we need to choose some units in which to express the volume. We choose our units so that the instanton size,  $\rho$ , is 0.2 in those units. That is

to say, our unit of length is  $5 \times \rho$ . These are the units we shall use throughout the present paper. We shall show the results of the finite volume study for a packing fraction of unity,  $f = 1$ . This is a value intermediate between the extremes of very high and very low density where our approach is certain to break down (as discussed earlier). It is a natural value to consider in the pure gauge theory, which has only one scale. Note that for  $f = 1$  a volume  $V = 1$  will contain  $n_{\bar{I}} + n_I = 126$  topological objects. In our calculations we shall, unless explicitly stated otherwise, use  $n_{\bar{I}} = n_I$  so that  $Q = 0$ , in the expectation (as discussed earlier) that this will minimise finite- $V$  corrections.

So, we have calculated the Dirac spectra for various values of  $V$  at  $f = 1$  and for  $Q = 0$ . We have fitted the small  $\lambda$  part of the spectrum to the form in equation 3. In figure 1 we show how the degree of divergence,  $d$ , varies with the volume  $V$ . In figure 2 we show the corresponding variation of the coefficient of the divergent term as a function of the volume (i.e.  $b$  in equation 3). We see that both quantities appear to have finite non-zero limits as  $V \rightarrow \infty$ , and that at  $V = 1$  the corrections are modest; so such a volume can be used to extract qualitative features of the spectrum. Although we do not show the full spectra we remark that finite- $V$  corrections are small across the whole range of  $\lambda$  and not just for  $\lambda \sim 0$ . We have also performed some calculations on different space-time volumes at other values of  $f$  and the conclusions, of these less systematic studies are in agreement with what we have found at  $f = 1$ . That is to say, finite volume corrections are small and, for our qualitative purposes, one can safely work on a space-time volume  $V = 1$  in our units.

The second question we ask is: how does the degree of divergence  $d$  depend on the packing fraction,  $f$ , as defined in equation 4? We perform our calculations on  $\mathbb{T}^4$  using hard sphere wavefunctions with  $Q = 0$  and on a volume  $V = 1$ . The results are shown in figure 3. We observe that there is a rapid decrease of  $d$  with increasing instanton density precisely in the range of densities that is of physical interest. Thus, while we can claim that the existence of a divergence is a characteristic feature of the instanton induced Dirac spectrum, the precise degree of divergence is not something that we can claim to predict with our model. We note that at very high densities the divergence effectively disappears. However,

since our model becomes unreliable in that limit we should be cautious about inferring that this is the case for the true spectrum. We also note that at very low densities the value of  $d$  will be determined by the detailed nature of the tail of the wave-function being used.

The calculations described above are specified in more detail in table I. We show there the  $\chi^2/N_{DF}$  (per degree of freedom) of the best fit. We have typically fitted the eigenvalue range  $\lambda \in [0, 0.3]$  where the best fits have  $\chi^2/N_{DF}$  between 1 and 2. (Note that with our choice of units, the maximum value of  $\lambda$  is about 5.0). In practice one can easily reduce the value of  $\chi^2/N_{DF}$  to less than unity by reducing the fitted range to about  $\lambda \in [0, 0.1]$ . The value of  $d$  is almost completely insensitive to which of these two ranges is chosen. In either case, the range of  $\lambda$  is substantial enough that the spectrum therein is determined with a high accuracy so that the fact that equation 3 fits well provides convincing evidence that we do indeed have a power-like divergence as  $\lambda \rightarrow 0$ .

To emphasise the last point further we have also fitted our  $\lambda \rightarrow 0$  spectra with a logarithmic divergence:

$$\bar{\nu}(\lambda) = a + b \ln(\lambda). \tag{28}$$

Typical best  $\chi^2/N_{DF}$  values are shown in table I. We see that such fits are quite unacceptable except at the higher densities where the divergence almost disappears,  $d \rightarrow 0$ . In that case the trivial expansion  $\lambda^{-d} \simeq 1 - d \ln(\lambda)$  explains the inevitable compatibility of both kinds of fits. We remark that a logarithmic divergence is of particular interest because of its appearance in quenched chiral perturbation theory [16] and it has been recently discussed in the context of Random Matrix Theory [17]. For a brief discussion of the possible connection between our power-like divergence and that in quenched chiral perturbation theory [18] we refer the reader to the concluding section of [10] and of this paper.

We now turn to two more complex questions: first, how robust are the qualitative features we have described above against changes in the functional form of the would-be zero-mode wavefunction, and second, are these features in some way special to our particular simplification of the Dirac operator?

First, the Dirac operator. One thing we can do (and the only thing we will do) is to see what happens if one goes one step ‘better’ than we have done so far and replaces the covariant derivative by the partial derivative as in equation 19. We use the ‘classical’ form for the zero-mode, as in equation 25. We then generate two ensembles (in  $\mathbb{R}^4$ ) with the same values of  $f$  and  $V$ . (They happen to be  $f \simeq 1$  and  $V \simeq 1$  but we have not yet discussed how we determine  $f$  and  $V$  for anything other than the hard-sphere wavefunction.) The first ensemble uses our usual simplification for the covariant derivative, as in equation 20. The second ensemble calculates the matrix element of the derivative using the approximate form given in equation 27. We compare the resulting Dirac spectra in figure 4 and table I (with the latter ensemble under the heading “Class. II”). We see that while there are some quantitative differences, as there must be, the qualitative features – chiral symmetry breaking and a divergence as  $\lambda \rightarrow 0$  – are certainly both there. Indeed the values of the degree of divergence as listed in table I are almost identical. This provides some non-trivial evidence that the qualitative features we are emphasising, do not in fact arise from our particular simplification of the covariant derivative.

How robust are our results against changing the wavefunction? A preliminary answer to this question is provided in figure 5. There we plot the spectral densities obtained with hard-sphere, Gaussian and classical zero-modes respectively, in a volume  $V = 1$  and with a packing fraction, of  $f = 1$  for the hard-sphere. We observe that they are indeed nearly identical.

Of course, this comparison skates over some points that need elaboration. Firstly, while the hard-sphere and Gaussian wavefunction calculations are in  $\mathbb{T}^4$ , the calculation with the classical wavefunction is in  $\mathbb{R}^4$ . Are the spectra obtained in  $\mathbb{T}^4$  and in  $\mathbb{R}^4$ , for a given wavefunction choice, similar enough for such a comparison to be useful? Of course they must become identical as  $V \rightarrow \infty$ ; but at  $V = 1$ ? To answer this question we show in figure 6 the spectral densities that one obtains with  $f = 1$ ,  $V = 1$  hard-sphere ensembles in  $\mathbb{T}^4$  and  $\mathbb{R}^4$  respectively. We observe that they are very similar. We thus conclude, from this and some similar comparisons, that a volume of  $V = 1$  is already large enough to allow

comparisons on these two, somewhat different space-time manifolds.

A second point concerns the ‘packing fraction’  $f$  of wavefunctions other than the hard sphere. We have seen that the hard-sphere Dirac spectrum varies rapidly with  $f$ , and so this is likely to be the case for the other wavefunctions. So ideally one would want to plot say  $d$  against  $f$  and see if the results were qualitatively the same for all wavefunctions. Unfortunately there cannot be a definition of  $f$  that is really equivalent for all the wavefunctions. So the best we can do is to see if one can actually find values of the size parameters  $\sigma$  and  $\omega$  such that the divergences obtained with Gaussian and classical wavefunctions are the same as the one obtains with hard spheres, for the chosen values of  $f$  and  $V$ . If that is the case – and if so it would represent a non-trivial result – then it will be interesting to see if the various ensembles possess some other properties that indicate that they are of a comparable density.

We therefore proceed as follows. We consider some hard sphere configurations, in a fixed volume  $V$ , fixed packing fraction  $f$  consisting of objects of a single size  $\rho$ . To be concrete let us choose  $V = 1$  (the unit four torus),  $\rho = 0.2$  and  $n_T + n_I = 63 + 63$  which gives  $f = 1$ . We extract the spectral density from these configurations and fit it using the power law form given in equation 3. We then generate configurations using a Gaussian wavefunction of size  $\sigma$  and with the same number of topological objects as before. The latter ensures that when  $\sigma$  is equivalent to  $\rho = 0.2$ , the volume will be  $V = 1$ . We now extract the spectral density, do a power law fit for  $\lambda \rightarrow 0$  and extract a value of the divergence exponent  $d$ . We repeat this for various values of  $\sigma$ . If we find a value for which  $d$  is the same as for the hard-sphere case, then we say that this is the equivalent value. (Note that when we vary  $\sigma$  we not only vary  $f$  but we also vary  $V$ . However we have seen for the hardsphere wavefunction that the variation of  $d$  on  $V$  is weak in comparison to its variation on  $f$ .) We repeat the above using the classical zero-mode. If we follow this procedure we find that  $\sigma = 0.074$  and  $\omega = 0.02$  are equivalent to  $\rho = 0.2$ . These values were in fact the ones used to generate the spectra shown in figure 5. Some properties of the various spectra are listed in table I. There we label the various ensembles by the ‘equivalent’  $f$  and  $V$  as determined above.



The fact that we tuned the size parameters  $\sigma$  and  $\omega$  so that they would give the same divergence as the hard sphere spectrum with  $\rho = 0.2$  does not mean that the comparison in figure 5 is in any way trivial. The fact that one can successfully perform such a tuning already shows that power-law divergences naturally arise with all these quite different wavefunctions. We also see in figure 5 that when we perform this tuning, the whole spectrum, and not just the divergent piece, is quite robust against changes in the wavefunction.

Using the above way of setting a common scale for the various wavefunctions, we can extend our earlier check of the  $V$  dependence of the divergent  $\lambda \rightarrow 0$  piece of the spectrum. We do this for the Gaussian wavefunction in figure 1. We see that the finite- $V$  corrections are very much as for the hard sphere. In figure 3 we show how  $d$  varies with the packing fraction  $f$  for the Gaussian. We see that, just as for the hard sphere, the divergence becomes weaker at higher densities. However the agreement is only qualitative. This means that if we had performed our ‘tuning’ to the hard-sphere spectrum at a different value of  $f$  than  $f = 1$ , then we would have obtained a somewhat different equivalent value of  $\sigma$ . This is inevitable since different wavefunctions are certainly not equivalent in all respects.

It is interesting to check, in some quite independent way, whether the above ‘equivalent’ sizes do really correspond to packing fractions that are very roughly comparable. Consider, for example, the total overlap of an instanton would-be zero-mode with all the anti-instanton would-be zero modes in the configuration. This will clearly increase linearly with the packing fraction (since the charges are positioned at random) and will be independent of  $V$  once  $V$  is large enough. So its value clearly provides a measure of the density that allows a crude comparison between different wavefunctions. We have calculated this integrated overlap for the hard-sphere, Gaussian and classical ensembles used in figure 5 and find values 0.496, 0.297 and 0.495 respectively. These are indeed similar enough to be reassuring.

## B. Realistic instanton ensembles

One might expect that a simple way to learn what actually occurs in quenched QCD, is to replace the artificial ensembles that we have been using, in most of which the instantons have a fixed size and number and are positioned at random, with the instanton ensembles extracted in actual lattice simulations [8,9]. Unfortunately such an approach possesses ambiguities both in principle and in practice. An example of the former is the question of how to separate the effect of topological from non-topological fluctuations; after all, the detailed features of the instanton ensemble will be in part due to such non-topological fluctuations. A practical difficulty one encounters [10] is the fact that the density of the lattice instanton ensembles turns out to be very sensitive to the smoothing of the gauge fields, which is necessary to remove the high-frequency fluctuations that would otherwise obscure the (lattice) topological charge density. Depending on how much smoothing one performs, one can obtain [10] spectral densities with or without a small- $\lambda$  peak.

That is not to say that calculations with realistic instanton ensembles don't have interesting lessons to teach us. For example one learns [10] that within an apparently dense instanton 'gas', the narrower instantons can contribute a small- $\lambda$  peak to the Dirac spectral density, just as though they were part of a much less dense gas. The reason for this phenomenon is simple [10]. The high packing fraction of the lattice instanton 'gas' is dominated by the very large instantons (since  $V_I \propto \rho^4$  in equation 4) but such instantons will have a small part of their wavefunction in the small region of space-time occupied by the wavefunction of a small instanton. Thus the matrix elements of  $i\not{D}$  between large and small instantons can be neglected to a first approximation, and the latter effectively interact as though they belonged to a much less dense gas of, on the average, smaller instantons. This observation is of particular interest because it (potentially) provides a justification for the use of relatively dilute gases of small instantons in various successful phenomenological studies [3].

In [10] the would-be zero mode wavefunctions used were hard spheres. However we have seen in this paper that while we can set up an approximate equivalence between different

wavefunctions by matching spectral densities or, more directly, the overlaps themselves, the actual scales characterising the matched wavefunctions are quite different. Since we have not determined which scale corresponds to a particular instanton size as determined in a lattice calculation, this again leaves a great deal of ambiguity in determining the corresponding packing fraction,  $f$ , since doing so would require determining the matched hard-sphere radius to be used in equation 4. This is an ambiguity of which the reader of [10] should be aware.

Indeed when we refer in this paper to the size of an instanton, for example  $\rho = 0.2$ , the reader should be aware that what we mean is that the instanton has such a size that its would-be zero mode can be approximated by a hard-sphere of radius  $\rho = 0.2$ . (That the real would-be zero-mode can be approximated by a hard sphere is suggested by the fact that we can match the spectral density from hard spheres with that from Gaussians or classical zero modes.) Its actual size, in terms of the spread of the topological charge density, may well be somewhat different, and trying to determine that (for the fully fluctuating vacuum of interest) lies well beyond the scope of the present work.

### C. Dynamics

We have provided evidence that the power-like divergence induced in the Dirac spectrum by instantons is not an artefact of the approximations used in our model but is a real effect. We can therefore begin to ask some questions about its dynamical origins. There are three issues we shall address. The first is whether there is any evidence for the simple picture [7] for the origin of this divergence that we presented in Section II. The second question is whether the divergence has an origin in the simplest two-body interactions between instantons and anti-instantons. Finally we ask whether the eigenvectors of the Dirac operator have any striking features as  $\lambda \rightarrow 0$ .

1. *Eigenvalue replacement hypothesis*

In Section II we described a simple scenario in which a divergent spectrum will naturally arise. In that argument one assumes that the only finite- $V$  correction in the (normalised) Dirac spectrum consists of a cut-off for  $|\lambda| \leq c/V$  (for some constant  $c$ ). If we increase the volume from  $V$  to  $V + \delta V$  then the (fractionally) greater number of modes in the interval  $|\lambda| \in [c/(V + \delta V), c/V]$  must match the fractional decrease in the number of exact zero-modes. This assumption that the fractional decrease in the exact zero modes is compensated for by an increase amongst the very smallest non-zero modes, we earlier referred to as the ‘eigenvalue replacement hypothesis’. As we saw, it leads to a divergent spectrum, as  $\lambda \rightarrow 0$ , with a power exponent  $d = 0.5$ . The fact that in practice we find that the power depends on the packing fraction tells us that this argument is approximate at best. It is interesting nonetheless to see if it does capture some of the essential features of what is happening.

A simple first step (which is as far as we shall try to go in this paper) is to determine whether our eigenvalue replacement hypothesis is qualitatively correct. Since this concerns the nature of the finite- $V$  corrections, we shall need to generate configurations with no constraint on the value of  $Q$ . Our strategy will be twofold. Firstly we generate configurations at a fixed packing fraction but for two volumes, and we check explicitly whether the finite volume corrections to the spectrum are really concentrated at small values of  $\lambda$ . Secondly we shall perform calculations at fixed  $V$  and compare, for example, configurations with  $Q = 0$  and  $Q = 2$  so as to see whether the extra 2 non-zero modes in the former are indeed concentrated amongst the lowest modes of the latter.

For our first calculation, the one with two different volumes, we draw the number of instantons and anti-instantons in each configuration from a normal distribution:

$$N_{I,A} \sim N(\bar{N}/2, \bar{N}/4) \tag{29}$$

where  $\bar{N} \propto V$  is the mean number of topological charges in the volume  $V$  (for instance we have  $\bar{N} = 126$  for  $V = 1$ ,  $f = 1$ ). We see therefore that the total number of objects

$N = N_I + N_A \sim N(\bar{N}, \bar{N}/2)$  and that the winding number distribution follows  $Q = N_I - N_A \sim N(0, \bar{N}/2)$ . (The actual numerical factors arise as this is nothing other than the central limit theorem applied to the binomial distribution  $N_{I,A} \sim B(\bar{N}, 1/2)$  for large  $\bar{N}$ .) The resulting Dirac spectra for such a gas in two different volumes is shown in figure 7 and is listed in table II. The results clearly show a far greater difference at small eigenvalues with the curves converging for  $\lambda \geq 0.04$ . (Note that the spectrum extends out to  $\lambda_{max} \sim 5$ .) This can be seen more clearly if we simply focus on the difference between the two spectral densities as in figure 8. This provides qualitative support for what we have called the eigenvalue replacement hypothesis.

As an aside, we note from table II that the value of  $d$  for ensembles where  $Q$  varies shows much stronger finite- $V$  corrections than for the  $Q = 0$  ensembles listed in table I. (As  $V \rightarrow \infty$  both ensembles should give the same value of  $d$ .) This shows that our earlier strategy of using  $Q = 0$  ensembles so as to minimise finite volume corrections was appropriate.

One way to go beyond the above qualitative analysis is as follows. Consider configurations with some fixed total number of charges i.e. in a fixed volume. We denote the un-normalised density of *non-zero* eigenvalues obtained from configurations with topological charge  $\pm Q$  by  $\rho(\lambda, |Q|)$ . Note that we explicitly exclude the exact zero-modes from this density. Its integral over the interval  $[\lambda_1, \lambda_2]$  is simply the average number of eigenvalues in that interval for such configurations. Let us now define a second density,  $\rho_{min}(\lambda, |Q|)$ , that counts only the smallest positive eigenvalue in each configuration. So its integral over  $\lambda \in [0, \infty]$  is just 1. Suppose we now simultaneously consider configurations with charge  $|Q|$  and  $|Q| + 2$ . The latter will have 2 extra zero-modes, i.e. the former will have one extra positive mode (and of course a corresponding negative mode as well). In this context the eigenvalue replacement hypothesis would say that the two extra zero-modes in the configurations with charge  $|Q| + 2$  replace the lowest positive (and largest negative) eigenvalues in the configurations with charge  $|Q|$ , i.e.

$$\rho_{min}(\lambda, |Q|) = \rho(\lambda, |Q|) - \rho(\lambda, |Q| + 2). \quad (30)$$

We shall test the following integrated form of this relation. The smallest eigenvalue is obviously localised at small  $\lambda$ . Define  $\lambda_0$  by

$$\int_0^{\lambda_0} \rho_{min}(\lambda, |Q|) = 0.98. \quad (31)$$

Thus the interval  $[0, \lambda_0]$  is essentially where the lowest positive eigenvalue is localised. (We have used 0.98 rather than 1 in equation 31 because formally at least there will be a non-zero, even if infinitesimal, probability for the smallest eigenvalue to be large.) We can now calculate the quantity

$$\delta\rho(|Q|, |Q| + 2) = \int_0^{\lambda_0} \{\rho(\lambda, |Q|) - \rho(\lambda, |Q| + 2)\}. \quad (32)$$

If the eigenvalue replacement hypothesis held exactly then we would expect this to be 0.98 for all  $|Q|$ . This test was performed in [12] using hard spheres and we quote the results of that calculation in table III. (In [7,12] the overlap calculation is cruder than ours, but that should not make a significant difference.) We observe from the table that the eigenvalue replacement hypothesis does indeed provide an approximately valid description. Typically about 80% of the difference between the  $|Q|$  and  $|Q| + 2$  spectra resides in the region occupied by the very lowest eigenvalue in the configurations with  $|Q|$ . We also note that as  $|Q|$  increases this percentage decreases. It is presumably this feature that leads to the power of the divergence not being precisely 0.5 and is what enables it to vary with the packing fraction. Thus, while the eigenvalue spectra do not satisfy the eigenvalue replacement hypothesis exactly, they do so approximately and it presumably provides a qualitative starting point for understanding the origins of the divergence.

## *2. Two body interactions*

In the case of hard-sphere wavefunctions, when the gas is sufficiently dilute that the chance for an instanton to overlap with more than one other charge may be neglected, it is easy to show analytically that the eigenvalue spectrum diverges as  $\lambda \rightarrow 0$  as  $1/\lambda^{0.6}$ . This

follows from the fact that if two hard spheres overlap by a small distance  $\delta$  then the overlap volume is  $\propto \delta^{\frac{5}{2}}$ . This will then be the eigenvalue shift from 0 due to the two body mixing. The probability measure is  $\propto d\delta$ , which, because  $\lambda \propto \delta^{\frac{5}{2}}$ , is just  $\propto 1/\lambda^{0.6}$ . Thus here the origin of the divergence is relatively trivial. The fact that our observed divergence appears for all the quite different wavefunctions that we have used, already tells us that its origin can hardly be so trivial. Nonetheless it does raise the question whether it is primarily due to 2-body dipole-like mixing, in which case it should be easy to understand, or to much more complex multi-body mixings. This is the question we shall now address.

We address this issue in two ways. Firstly we generate a ‘background spectral density’ consisting of simple pairwise splittings of eigenvalues. Secondly, we explicitly construct a gas of dipoles and see if we still find a peak at small eigenvalues.

Figure 9 shows the spectral density for the hard sphere wavefunction coming from the actual eigenvalues of our Dirac matrix. It also shows a ‘background curve’ which originates from pairwise interactions between the topological charges in the same ensemble calculated as follows. Consider a configuration with  $Q = 0$ . We go through the set of instantons and for each one find the largest overlap with a neighbouring anti-instanton. We then use this overlap in a 2-body mixing matrix to obtain the eigenvalue shift from zero:

$$\lambda_i = \pm \max_j \{V_{ij}\} \tag{33}$$

This then produces for us the ‘background spectral density’ plotted in figure 9. We remark that if we had  $Q < 0$  then we would again go through the  $n_I$  instantons, associating each with two eigenvalues, symmetrically split about zero, as above. The rest of the eigenvalues are zero by the the Atiyah-Singer theorem. Analogously for  $Q > 0$ . The background curve thus generated only takes into account pairwise splitting and furthermore ignores totally the effects of other objects of the same charge in the vicinity. We see that the  $\lambda \rightarrow 0$  peak does not appear in the background curve. This indicates that the  $\lambda \rightarrow 0$  peak that we observe in the Dirac spectrum is not due a simple 2-body interaction.

There are many ways to produce such a background curve, so this example cannot be

considered conclusive. For example one might try to produce a background curve just as above except that any anti-instanton that is used once in a 2-body mixing cannot be used again; it is effectively removed. This produces a quite different spectrum, which has a plethora of extra near-zero and exactly zero eigenvalues. This is because, as we remove anti-instantons from the configuration, we are soon left with a very dilute gas of topological charges. This is clearly an artefact of the procedure, but serves to illustrate the inherent ambiguity in trying to generate a background curve.

To further explore this question we explicitly construct a  $Q = 0$  ensemble of topological charges from a gas of dipoles, pairing off each object with one of the opposite chirality. We use hard sphere wavefunctions of size  $\rho$  and the distance between the opposite charges within each dipole is chosen at random (with a four-volume weighting) within some interval  $|x^+ - x^-| \in [0, r_{max}]$  for some  $r_{max}$ . If  $r_{max} < 2\rho$  then the dipoles will always have a non-zero overlap and we would naively expect no eigenvalues near zero if only 2-body interactions are important. In figure 10 we show the spectrum for such a gas of dipoles in the case where  $r_{max} = 2\rho$ . We compare it to the spectrum one obtains with a  $Q = 0$  gas of (anti)instantons placed at random in the volume. We also show the background spectrum that one obtains by calculating the eigenvalues of the dipole gas, from the mixing within each dipole taken in isolation. (Note that this may differ somewhat from our previously defined background spectrum.) We observe that the dipole gas spectrum is far from the background curve and not so different to that of the randomly placed charges. This shows that the eigenfunctions corresponding to the small modes in the divergent peak, are formed by a mixing that is very far from simple two body.

An even more striking example is provided by choosing  $r_{max} = \rho$ . Now the minimum overlap is very large and we would naively expect the spectrum to have no small eigenvalues at all. In figure 11 we show the background curve obtained by treating each dipole in isolation, and indeed it possesses a sharp cut off as expected. Remarkably enough, however, the actual Dirac spectrum we calculate from this gas of heavily overlapping dipoles does possess a non-zero density of modes at  $\lambda = 0$  and hence breaks chiral symmetry spontaneously. This



shows that there is a component to the mixing that is far from simple two-body, and it is this component that drives the spontaneous breaking of the chiral symmetry.

### 3. The eigenfunctions for $\lambda \rightarrow 0$

It would obviously be interesting to learn something about those eigenfunctions of the Dirac operator that correspond to the small eigenvalues that drive chiral symmetry breaking. We have seen above that their origin lies in something more complex than simple two-body mixing. Since chiral symmetry breaking is associated with the presence of a massless Goldstone boson, the pion, one might expect that the eigenfunctions would become more extended as  $\lambda \rightarrow 0$ ; perhaps, even, that the extent of these eigenfunctions might diverge. If this were so, then this could perhaps be linked to the masslessness of the pion using the standard decomposition of the component quark propagators in terms of the eigenvalues and eigenfunctions of the Dirac operator [19].

To explore this question we need a measure of the dispersion of the eigenfunction  $|e_\lambda\rangle$  corresponding to the eigenvalue  $\lambda$  of our Dirac operator, i.e.  $i\mathcal{D}|e_\lambda\rangle = \lambda|e_\lambda\rangle$ . We first define the function

$$R(x_c) = \langle e_\lambda | (x - x_c)^2 | e_\lambda \rangle, \quad (34)$$

that is clearly a measure of the dispersion around the point  $x_c$ . The extent space-time of the eigenfunction is provided by the dispersion about the ‘centre-of-mass’. Since the dispersion is minimised when we choose  $x_c$  to be the ‘centre-of-mass’, we can calculate the extent of the eigenvector directly by

$$D = \min_{x_c} R^{1/2}(x_c). \quad (35)$$

In practice we do these calculations by decomposing the eigenvector  $|e_\lambda\rangle$  into a linear combination of the would-be zero-modes and working out the dispersions of these using, where appropriate, some simple approximations.

We have performed a calculation with an ensemble of hard-spheres on volumes  $V = 0.41, 1.0, 1.5$ . The results of  $D(\lambda)$  for these three volumes is shown in figure 12. We see that the dispersion increases with decreasing eigenvalue; perhaps roughly linearly. We also see that there are stronger finite volume effects at smaller values of  $\lambda$ . It would appear that the eigenvectors for small  $\lambda$  are being constrained by our finite volumes to be smaller than they would otherwise be. Whether the dispersion would actually diverge at  $\lambda = 0$  in the  $V \rightarrow \infty$  limit is a question we obviously cannot answer. Certainly this shows that the modes that are important for the spontaneous breaking of chiral symmetry are delocalised on the scale of instanton nearest-neighbour interactions. The implications of figure 12 are intriguing and need further investigation.

## V. FULL QCD ( $N_F=1,2$ )

In this section we shall use the simplest hard-sphere version of our model to analyse QCD with 1 and 2 quark flavours. The calculations are, computationally, far more intensive than for the pure gauge theory, and we will not be able to perform the various checks that we were able to perform in that case. Thus, although we are reassured by the fact that this simplest hard-sphere analysis proved remarkably robust in quenched QCD, we must regard the calculations here as being of an exploratory nature.

There is a surprisingly large number of non-trivial questions we can ask within the framework of our model. We shall focus upon:

- Spectral density. How does the spectral density behave with dynamical quarks? Do we still get a power divergence as seen previously,  $b(m)\lambda^{-d(m)}$  where  $b(m)$ ,  $d(m)$  are now dependent upon the quark mass? What is the behaviour of the spectral density as a function of the number of quark flavours  $N_f$ ?
- Chiral condensate. What is the behaviour of  $\langle \bar{\psi}\psi \rangle(m)$ ? In particular, do we have spontaneous symmetry breaking and how does it behave as a function of the number of quark flavours?

- Topological susceptibility. General arguments give the behaviour of this quantity as:

$$\begin{aligned} \langle Q^2 \rangle &\propto mV && \text{symmetry broken phase} \\ &\propto m^{N_f}V && \text{symmetric phase.} \end{aligned} \tag{36}$$

Can our model reproduce such behaviour ?

- Particle masses. In particular, does the mass of the  $\eta'$  meson go to a non-zero limit as the quark mass  $m \rightarrow 0$  ?

We shall begin by describing in detail how we generate the instanton configurations for  $N_f \neq 0$ . We then describe how we calculate the  $\eta'$  and  $\sigma$  masses in our model. From there we move on to our calculations, in which we address the questions listed above.

### A. Ensemble generation

The weighting of the instanton ensembles will have a gauge part and a fermionic part. The gauge part will be the same as in the quenched case, except that we will allow both  $Q$  and  $N$  (the total number of topological charges) to vary. We vary  $Q$  because we want to calculate the  $m$ -dependence of  $\langle Q^2 \rangle$ . In addition we expect that  $\langle Q^2 \rangle$  will cease to be large once  $m$  is small, and then there is the danger that using only  $Q = 0$  will bias the physics. The reason for varying  $N$  is less compelling and, in practice, the main purpose of such calculations will be as a check on our more extensive fixed- $N$  calculations.

#### 1. The gauge weighting

As in the quenched case, the topological charges are positioned at random in space-time, with a fixed size ( $\rho=0.2$ ). When we wish to allow  $N = N_A + N_I$  to vary, we choose the number of instantons using a Poisson distribution, and the same for anti-instantons. The two distributions are taken to be independent:

$$P(N_A = s, N_I = t) = \exp(-2\mu) \frac{\mu^{s+t}}{s!t!} \tag{37}$$

Note that  $\mu$  would be the mean number of instantons (as well as of anti-instantons) if we used the gauge weighting alone. (This is similar to equation 29 with  $\mu = \bar{N}/2$ , albeit with a different variance.)

## 2. The fermion weighting

In the case when  $N = N_A + N_I$  is fixed, the obvious fermion weighting to use is one that is calculated entirely within the basis of would-be zero modes,

$$\det(i\mathcal{D}[A] - im) \doteq m^{|N_A - N_I|} \prod_{i=1}^{\min(N_I, N_A)} (\lambda_i^2 + m^2) \quad (38)$$

(raised to the power  $N_f$ ) where the  $\lambda_i$  are the eigenvalues we obtain, for the given instanton ensemble, as described earlier in this paper. There are of course other modes but their number does not change, since the total number of modes  $N_T$  is fixed if we are in a fixed volume (with a fixed ultraviolet cut-off). We have assumed, in our calculations of the chiral condensate, that it is a good approximation to neglect the variation of these other modes as we alter the instanton gas, and equation 38 embodies the same assumption.

If, however, we vary  $N = N_A + N_I$  then we can no longer ignore these other modes: their number,  $N_T - N$ , will vary and so some choice has to be made for their weighting. We will make the simplest choice: each mode will be set to a fixed value  $\bar{\lambda}_{NZ}$ . In that case our weighting becomes

$$\det(i\mathcal{D}[A] - im) \doteq (\bar{\lambda}_{NZ}^2 + m^2)^{(N_T - N_A - N_I)/2} m^{|N_A - N_I|} \prod_{i=1}^{\min(N_I, N_A)} (\lambda_i^2 + m^2) \quad (39)$$

(again raised to the power  $N_f$ ). It is clear that we do not actually have to choose a concrete value for  $N_T$  since it is only the ratio of the determinants that enters into the probability of changing one configuration of instantons for another one, and in the ratio the factor  $(\bar{\lambda}_{NZ}^2 + m^2)^{N_T/2}$  drops out. However we do need some choice for the value of  $\bar{\lambda}_{NZ}$ . In keeping with our assumption that the lowest-lying eigenvalues are generated by the mixing of the would-be zero modes, we shall choose  $\bar{\lambda}_{NZ}$  to be somewhat larger than the average

eigenvalue in the zero-mode basis. A typical quenched QCD eigenvalue spectrum is shown in figure 13, and this has an average eigenvalue of  $\bar{\lambda} \simeq 1.1$ ; so we shall choose  $\bar{\lambda}_{NZ} = 2.0$  in our calculations. The somewhat arbitrary nature of this choice is unsatisfactory and in practice we shall minimise the ambiguity by only performing such calculations for  $m \ll \bar{\lambda}_{NZ}$ . (We remark that in our Monte Carlo we have actually used  $(\bar{\lambda}_{NZ} + m)$  rather than  $(\bar{\lambda}_{NZ}^2 + m^2)^{1/2}$ ; but for  $m \ll \bar{\lambda}_{NZ}$  this should not matter.) Most of our calculations will be for fixed  $N$ . In this case the values of  $Q$  are necessarily all even or all odd. This should not introduce a significant bias as long as  $\langle Q^2 \rangle$  is not too small.

### 3. Monte Carlo simulation

As described above, we incorporate a gauge and fermion weighting into our model using the two parameters  $\mu$  and  $\bar{\lambda}_{NZ}$ . The parameter  $\mu$  is related to the packing fraction of our configurations but does not determine it wholly because the fermion determinant will also play a part in finding the equilibrium number of objects in the gas.

The Monte Carlo simulation begins with a random configuration. We then move a single object to generate a new trial configuration. This process is repeated as we “sweep” through the gas, moving each object in turn, accepting moves according to the standard Metropolis algorithm:

$$\begin{aligned}
 P(\text{accept}) &= 1 && \det(\text{new}) > \det(\text{old}) \\
 &= \left\{ \frac{\det(\text{new})}{\det(\text{old})} \right\}^{N_f} && \text{otherwise.}
 \end{aligned}
 \tag{40}$$

Periodically (usually every 10 attempted moves) we attempt to either increase or decrease the number of instantons or anti-instantons by one. We expect the system to come into equilibrium after some number of sweeps. As the change between successive configurations is small (differing only in the position of a single object or in having one extra or one fewer object), we clearly require long sequences of configurations, both to thermalise and to obtain a useful number of effectively independent configurations. Whilst we use all the

configurations that we generate (after equilibration) our statistical analysis uses a binned jack-knife procedure that should ensure reasonably accurate error analyses.

To ensure thermalisation we monitor the values taken by  $N = N_I + N_A$  and  $Q = N_I - N_A$  during the sequence of instanton configurations generated by the Monte Carlo. In practice we find that a sequence of 630000 configurations appears to be sufficient to explore the available phase space; and that after 63000 configurations we appear to have thermalised (i.e. lost all memory of the random starting configuration). This is illustrated in figure 14 and figure 15 for the lightest quark mass we use, and in figure 16 and figure 17 for an intermediate quark mass. As one would expect the phase space is explored more weakly for the lighter mass.

## B. Calculating masses

The usual way to calculate masses in a (Euclidean) field theory is from the  $t$ -dependence of appropriate correlation functions. The latter can be estimated by standard Monte carlo techniques. We can attempt to apply the same approach to our instanton ensembles. Since we calculate the eigenvalues (and can easily calculate the corresponding eigenvectors) of  $i\mathcal{D}$ , we can, in principle, calculate quark and hence hadron propagators. Here, however, we shall limit ourselves to calculations that involve only ‘gluonic’ operators. That is to say, we calculate the masses of flavour-singlet mesons. This includes what is perhaps the most interesting meson in this context, the  $\eta'$ . We shall also calculate the mass of the scalar  $\sigma$ .

The  $\eta'$  has quantum numbers  $0^{-+}$  which are also the quantum numbers of the topological charge density. Thus it can be calculated from the correlation function,  $\langle Q(0)Q(t) \rangle$ , assuming the usual decomposition

$$\langle Q(0)Q(t) \rangle = \sum_n c_n \exp(-M_n t). \quad (41)$$

The lowest mass should be the  $\eta'$ . In practice what we do is to divide up our volume into a number of “strips” each of width  $\delta t \ll 1$ . We calculate the total ‘charge’ in a given strip

simply by adding up the charges of all the objects whose centres are contained within the strip. We call this  $Q(t)$  for the strip  $[t, t + \delta t)$ . That is to say,  $Q(t) = N_I(t) - N_A(t)$  where  $N_{I/A}(t)$  are the number of instantons/anti-instantons whose centres are contained within the strip. This differs from the actual topological charge density within a strip, but is clearly an equally good operator. (The difference is due to the spread of the instanton core; but that is modelled by some relatively arbitrary function within our model and so there is no point in including that.)

One might worry that the lightest mass contributing to the correlator in equation 41 might be a  $0^{-+}$  glueball rather than the  $\eta'$ . However we note that in the pure gauge theory the topological charges are completely uncorrelated, so the correlation length is zero, i.e. the  $0^{-+}$  glueball mass is  $\infty$ . Thus it seems safe to assume that it can be ignored in full QCD as well.

The  $\sigma$  has quantum numbers  $0^{++}$  and so can be calculated from correlators of the gluonic action density,  $\langle S_g(0)S_g(t) \rangle$ . Within our model the gluonic action density is simply proportional to the density of topological charges and so we use the correlator of  $N(t) = N_I(t) + N_A(t)$ , i.e. the total number of charges whose centres are located within the strip labelled by  $t$ . For the same reason as in the case of the  $0^{-+}$ , we can ignore the glueballs. However there is now a non-trivial vacuum state contribution, and so we have to use the vacuum subtracted correlator,  $\langle N(0)N(t) \rangle - \langle N(0) \rangle^2$ . The large- $t$  exponential fall-off of this correlator should then give us the mass of the  $\sigma$  meson. (Note that if we fix  $N$  in our calculation, this induces long-range correlations that are not due to particle exchange. For this reason we do not calculate the  $\sigma$  mass in our fixed- $N$  calculations.)

To make sure that one has identified the large- $t$  exponential decay of a correlation function, it is useful to define an effective mass

$$m_{eff}(t) = -\ln \left( \frac{\langle \mathcal{O}(0)\mathcal{O}(t) \rangle}{\langle \mathcal{O}(0)\mathcal{O}(t-1) \rangle} \right), \quad (42)$$

where we have written our correlator with a generic operator  $\mathcal{O}$  which can represent either the charge or the number density. It should be apparent that if the correlation function

is in fact given by a simple exponential for  $t \geq t_0$  then our effective mass  $m_{eff}(t)$  will be independent of  $t$ , within errors, for  $t \geq t_0$ . If  $t_{min}$  is the smallest value of  $t_0$  for which this is the case, then  $m_{eff}(t_{min})$  provides us with an estimate of the lightest mass, and its error.

It is of course the case that our model is not a field theory and a decomposition of the kind given in equation 41 may not hold. However, since our model is intended to provide an approximation to the relevant infrared physics of QCD, we will take the masses we calculate in this way as being analogues, within our model, of the corresponding masses in QCD.

### C. Calculations

We perform calculations for both 1 and 2 quark flavours. For  $N_f = 1$  one expects no Goldstone boson since the one would-be Goldstone boson, the  $\eta'$ , acquires a mass through the anomaly. (For simplicity we shall refer to the flavour singlet pseudoscalar as the  $\eta'$  even though that is, strictly speaking, the flavour singlet member of the nonet with  $N_f = 3$ .) Although the  $U(1)$  chiral symmetry is broken by the anomaly, it is still interesting to see whether the Dirac spectrum possesses a non-zero  $\lambda \rightarrow 0$  limit. The  $N_f = 2$  case, on the other hand, contains essentially all the features of the physically relevant  $N_f = 2 + 1$  case.

We will carry out calculations separately for  $N$  fixed and for  $N$  being allowed to vary. The latter calculations will show that  $\langle N \rangle$  varies weakly with the quark mass  $m$ ; in contrast to  $\langle Q^2 \rangle$ . This suggests that constraining  $N$  to be fixed is not a serious bias. Most of our calculations will in fact be for  $N$  fixed, with the variable  $N$  calculations serving as a check. Fixing  $N$  has the advantage that we can avoid our rather ad hoc representation of the non-zero modes through an average eigenvalue,  $\bar{\lambda}_{NZ}$ . In addition we can see from figures 14- 17 that the Monte Carlo explores the fluctuations in  $N$  much more slowly than the fluctuations in  $Q$ . Thus a fixed- $N$  calculation may also prove to be statistically more accurate.

All the calculations described here will be with hard-sphere wavefunctions with radius  $\rho = 0.2$  and in a space-time volume  $V = 1$ . Our fixed  $N$  calculations will contain  $N = 126$  which corresponds to a packing fraction  $f = 1.0$ . When we vary  $N$  we choose the gauge



weighting so that the average value of  $N$  would be 126 if there were no fermionic weighting. In practice the latter reduces  $\langle N \rangle$  so that the packing fraction lies in the interval  $f \in [0.35, 0.55]$ .

For the calculations at fixed  $N$ , we choose quark masses  $m = 0.15, 0.3, 0.5, 1.0, 2.0$  and  $3.0$ . For the calculations with varying  $N$  we only use the lowest 3 values of  $m$ . This is because the fermionic weighting will presumably become sensitive to the precise value of  $\bar{\lambda}_{NZ}$  once  $m$  becomes comparable to it.

We expect that in our finite volume, we will lose chiral symmetry breaking once  $m$  becomes too small. To gain some intuition as to when that might occur, it is useful to express everything in physical ‘MeV’ units. If we take the instanton radius to be about  $0.5fm$  [8] then the length of our space-time, being  $5 \times \rho$ , is about  $2.5fm \simeq 1/80MeV$ . So  $m = 1$  corresponds to  $m = 80MeV$ , i.e. just a little lighter than the strange quark mass, and  $m = 0.15$  corresponds to  $m \simeq 12MeV$ , i.e. close to the physical  $u, d$  masses. Thus we should certainly not be surprised to see finite- $V$  effects at the lower end of our range of masses.

We now turn to the detailed results of our calculations, the parameters of which are summarised in table IV.

*1.  $N_f = 1$ ; variable  $N$ .*

In figure 18 we display the spectral density of the Dirac operator for quark masses,  $m = 0.15, 0.3, 0.5$ . The first thing we note is that the spectral density appears to diverge as  $\lambda \rightarrow 0$  for all three masses. It is however, equally clear that the spectral density is not independent of the quark mass. Indeed, if we fit the spectra to the power-law form in equation 3 then we find, as shown in table V, that the coefficient of the divergence appears to vanish,  $b \rightarrow 0$ , as  $m \rightarrow 0$ . Thus the divergence in the spectral density need not lead to a divergent quark condensate of the kind that we encountered in quenched QCD. This appears to be confirmed by a direct calculation of the chiral condensate against  $m$ , as shown in figure 19, where we see that we appear to have chiral symmetry breaking with a finite

condensate.

We also calculate  $\langle Q^2 \rangle$  as a function of  $m$ , and list the values in table IV. As we see from figure 20 the variation of  $\langle Q^2 \rangle$  is approximately linear with  $m$  in accord with what we expect from the anomalous Ward identities for QCD:

$$\frac{\langle Q^2 \rangle}{V} = \frac{m \langle \bar{\psi} \psi \rangle}{N_f^2} + O(m^2). \quad (43)$$

Indeed, if we insert into this equation the values relevant to our simulations, i.e.  $V = 1$ ,  $N_f = 1$  and the value for  $\langle \bar{\psi} \psi \rangle$  shown in figure 19, then we obtain predicted values for  $\langle Q^2 \rangle$  that are within  $\sim 25\%$  of the values shown in figure 20. This is quite remarkable.

We now turn to our calculation of the flavour singlet meson masses. In figure 21 we show an example of the correlation functions from which we extract the  $\eta'$  and  $\sigma$  masses. We can use equation 42 to extract effective masses, as shown for the  $\eta'$  in figure 22. The errors are large and there is not really much evidence that  $m_{eff}(t)$  plateaus at large  $t$  to a finite mass,  $m_{\eta'}$ . In this particular case we choose the effective mass at  $t = 0.1$  as our estimate of  $m_{\eta'}$  since, roughly speaking, effective masses at larger values of  $t$  are consistent with it within errors. We list in table V our mass estimates, obtained in this way. Despite the crudity of our calculation it seems clear that  $m_{\eta'}$  does not vanish as  $m \rightarrow 0$ : the  $\eta'$  is not a Goldstone boson. In our units, where  $\rho = 0.2$ , we find  $m_{\eta'} \sim 12$ . If we transform to ‘MeV’ units, using  $\rho \sim 0.5fm$ , then this mass becomes  $m_{\eta'} \sim 1GeV$ . In QCD this mass is generated by topological fluctuations, and through large- $N_c$  arguments can be related to the value of  $\langle Q^2 \rangle$  in the quenched theory. With our gauge weighting we would obtain in the quenched theory  $\langle Q^2 \rangle = N = 126$  and hence, in ‘MeV’ units,  $\langle Q^2 \rangle / V \sim (260MeV)^4$ . This is not so far from the true value [8] in quenched QCD,  $\sim (200MeV)^4$ , and shows that our model is doing remarkably well in reproducing the link between topology and physics in full QCD.

In table V we also list our estimates of the mass of the  $\sigma$ . It is comparable in mass to the  $\eta'$ , although perhaps slightly lighter.

2.  $N_f = 1$ ; *fixed*  $N$ .

The results of our calculations at fixed  $N$  are summarised in tables IV and V. Since the packing fraction is larger than for the variable- $N$  calculations (126 topological charges per unit volume versus  $\sim 70$ ) we do not expect agreement even in the common  $m$ -range. However the qualitative agreement is quite satisfactory. In figure 23 we plot the spectral density in this mass range and we see the same features as we saw in figure 18. The chiral condensate is plotted in figure 24. We see that there is a finite condensate as  $m \rightarrow 0$ , but that it is larger than the one shown in figure 19. However the factor by which it is larger is close to the trivial factor of  $\sim 126/70$  (the ratio of the number of charges). As for  $\langle Q^2 \rangle$ , we see an approximate linear decrease for  $m \leq 1.0$ . The actual value is larger than for the variable- $N$  case although by less than the factor of  $\sim 126/70$ . (One would only expect precisely this factor in the dilute gas limit.) For larger values of  $m$  the linear increase must flatten off, as it does, because it must approach the quenched ( $m \rightarrow \infty$ ) value of  $\langle Q^2 \rangle = N = 126$ . The calculated values of the  $\eta'$  mass, as shown in figure 25, are consistent with those obtained previously (and confirm that the  $\eta'$  is indeed not a Goldstone boson). All this confirms our expectation that fixing  $N$  does not alter the physics of the model in any significant way.

The larger range of  $m$  gives us a clearer perspective on the  $\propto b/\lambda^d$  divergence in the spectral density. We see from table V that the power  $d$  is independent of  $m$  except at the very smallest value of  $m$ . We provisionally ascribe this to a finite volume effect. (The reason for doing so will become clearer once we present the  $N_f = 2$  calculations.) We note that the value of  $d$  is smaller than the one we obtained for the variable- $N$  calculation. Since the packing fraction of the latter is smaller, this mirrors what we found in quenched QCD: the divergence weakens with increasing instanton density. Although  $d$  appears to be independent of  $m$ , this is clearly not the case for the coefficient  $b$ . In fact, in the intermediate mass range,  $m \in [0.3, 1.0]$ , the dependence of  $b$  is consistent, within errors, with  $b(m)/\lambda^{d(m)} = b_0(m/\lambda)^{d_0}$  as suggested by the simple argument leading to eqn 10.

### 3. $N_f = 2$ ; variable $N$ .

The spontaneous breaking of chiral symmetry that we found for  $N_f = 1$  is academic since the symmetry is in any case anomalous. We now turn to the corresponding  $N_f = 2$  calculations where there is a non-anomalous part of the chiral symmetry that may be spontaneously broken.

Before proceeding, a note of warning. It is of course trivial to vary the number of fermion flavours: all that is required is to take the ratio of the determinants to the power  $N_f$  in the Metropolis step. Not surprisingly, however, this makes the exploration of the available phase space much slower. This is illustrated in figure 26 where we show the total number of topological objects in a Monte Carlo generated sequence of configurations at our lowest mass value,  $m = 0.15$ . The corresponding plot for  $N_f = 1$  was shown in figure 14. The variation of  $N$  is very much slower in the case of 2 flavours. It is clear that if we want to go to smaller masses or larger values of  $N_f$  we shall need either much longer Monte Carlo sequences or improved algorithms. This point is further emphasised by figure 27 which displays the increasing difficulty in moving between sectors of different net topological charge.

The  $N_f = 2$  calculations with variable  $N$  have been performed for masses  $m = 0.15, 0.3, 0.5$  (chosen, as before, so that  $m \ll \bar{\lambda}_{NZ}$ ). The spectral densities for these three masses are depicted in figure 28. A quick comparison with figure 18 indicates that something very different is occurring for two flavours of fermions. The spectral density is much smaller in magnitude, and decreasing rapidly as  $m \rightarrow 0$ : all the signs of chiral symmetry restoration. This is highlighted by a direct comparison of the  $N_f = 1$  and  $N_f = 2$  spectra at  $m = 0.15$ , as shown in figure 29. And indeed, when we calculate the chiral condensate from the  $N_f = 2$  spectral densities, we obtain a condensate, as shown in figure 30, that is quite clearly vanishing as  $m \rightarrow 0$ .

We also calculate  $\langle Q^2 \rangle$ , as listed in table IV. If we plot the values versus  $m$ , as in figure 31, we see that the dependence is not linear, as one would expect in the phase with symmetry breaking, but rather is roughly  $\propto m^{N_f} = m^2$  as one would expect in the chirally

symmetric phase.

Our calculations are thus consistent with the theory being in a phase with explicit chiral symmetry. Now, while one does indeed expect to find chiral symmetry restoration as we increase  $N_f$ , it is not expected to occur before  $N_f = 6$  or so [20]. So if it already happens in our calculations for  $N_f = 2$  this would suggest that our model provides a rather poor representation of the fermionic physics in QCD.

There is another possibility: that for  $m \leq 0.3$  we have been driven by finite-volume effects into a symmetry restored phase. A mass of  $m = 0.3$  corresponds to  $m \sim 25MeV$  (using our usual criterion for converting to physical units) and this is surely small enough, in a volume  $V \sim 2.5fm^4$ , to lead to strong finite size effects. Moreover, such a change of phase has been observed in lattice QCD simulations [21]. To explore this possibility we need to perform calculations for larger  $m$ . Since we are reluctant to use  $m \sim \bar{\lambda}_{NZ}$ , we now turn to the fixed- $N$  calculations.

#### 4. $N_f = 2$ ; fixed $N$ .

Our fixed  $N$  calculations are performed over the range  $m \in [0.15, 3.0]$ . In the mass range  $m \leq 0.50$  we find the same qualitative behaviour as we obtained in the variable- $N$  calculations. However, when we compare the  $m = 0.15$  and  $m = 3.0$  spectra, as in figure 32, we immediately see a great difference between the two: the spectra corresponding to the smaller mass shows the depletion of eigenvalues at small  $\lambda$  that we expect to see if chiral symmetry is to be restored (compare with figure 29); the spectrum corresponding to  $m = 3.0$  shows no such depletion.

We integrate the spectra for the various masses, and plot the resulting chiral condensate in figure 33. This figure appears to confirm our speculation that chiral symmetry restoration is a small- $m$  finite volume effect. For  $m \geq 1.0 \sim 80MeV$  we have a chiral condensate that appears to be heading towards a non-zero  $m = 0$  intercept. For  $m < 1.0$  there is a sudden and drastic suppression. Such a behaviour is what one would expect if the restoration of chiral

symmetry were due to finite volume effects. The corresponding plot of  $\langle Q^2(m) \rangle$  is given in figure 34. We see an approximately linear behaviour for the larger quark masses, as we would expect for chiral symmetry breakdown, and, approximately quadratic behaviour for the smaller quark masses as before (see figure 31). All this strongly suggests that instantons do indeed break chiral symmetry for two flavours, but that finite volume effects set in earlier than with one flavour. Of course, one really needs to perform such calculations on larger volumes, in order to render this plausible scenario completely convincing.

We note that all the  $N_f = 2$  spectral densities have a power-like divergence at  $\lambda = 0$ . The parameters of the fits to  $b/\lambda^d$  are listed in table V. For those values of  $m$  where we have chiral symmetry breaking the power of the divergence appears to be  $d \simeq 0.3$  as for  $N_f = 1$ . As we enter the range of  $m$  where chiral symmetry is restored, the value of  $d$  increases, and the coefficient  $b$  decreases very rapidly. (Note that this supports our earlier suggestion that our  $N_f = 1$  calculation with  $m = 0.15$  is afflicted by similar finite- $V$  effects.) There is some evidence from the  $m = 1.0$  and  $2.0$  fits that  $b(m)/\lambda^{d(m)} = b_0(m/\lambda)^{d_0}$  as for  $N_f = 1$ .

Our estimates for the  $\eta'$  mass are listed in table V. We see that for values of  $m$  where we observe the spontaneous breaking of chiral symmetry, the mass is very similar for  $N_f = 1$  and  $N_f = 2$ . The restoration of chiral symmetry is associated with  $m_{\eta'}$  becoming much heavier (and, indeed, much harder to estimate reliably).

## VI. CONCLUSIONS

We have used a simple model for the way instanton zero-modes mix with each other, in order to learn how topology contributes to the Dirac spectral density, particularly at the small eigenvalues that are relevant to chiral symmetry breaking. We have done so for quenched QCD and for full QCD with both one and two flavours.

We have found that instantons do indeed appear to break chiral symmetry spontaneously, both in quenched QCD and in full QCD. We also found that the topological susceptibility appears to vanish linearly with the quark mass  $m$ , as required by the QCD anomalous Ward

identities when in a phase with chiral symmetry breaking. It is remarkable that our simple model manages to capture the subtle trade-off between exact zero-modes and the chiral symmetry breaking modes arbitrarily close to zero, which underlies this result.

That instantons should contribute to chiral symmetry breaking is not unexpected [1–3]. Our second result is less conventional. We find that the Dirac spectral density one obtains from instantons has a powerlike divergence as  $\lambda \rightarrow 0$ . In quenched QCD this  $\sim 1/\lambda^d$  behaviour translates into a pathological  $1/m^d$  divergence in the chiral condensate. In the case of full QCD the divergence is pushed to smaller eigenvalues as  $\lambda \rightarrow 0$ , perhaps having the form  $(m/\lambda)^d$ , and the chiral condensate is well-behaved. Nonetheless such a divergence means that the  $\lambda \rightarrow 0$  and  $m \rightarrow 0$  limits need special care, thus undermining, for example, the usual Banks-Casher relation.

These conclusions broadly confirm the results of earlier work [7,12] which used (essentially) the same model. The most important way in which we have extended that work, at least for quenched QCD, is to show, by varying the various components of the model, that the divergence appears to be a generic feature of instanton mixing. In addition, we have also shown that the strength of the divergence depends on the instanton density, becoming negligible for very high densities. In fact it seems that ‘realistic’ instanton ensembles, as produced via lattice simulations [8], fall precisely in the intermediate range of densities where the strength of the divergence is varying most rapidly [10]. Thus we are not able to predict the precise phenomenological impact of this divergence upon quenched QCD. However it is interesting that when we calculate the instanton mixing within these lattice ensembles, we find that the smaller instantons contribute disproportionately to the smallest eigenvalues; as though they were part of a more dilute gas. This may provide the crucial link between the rather dense gases of large instantons that many lattice studies obtain, and the much more dilute gases of significantly smaller instantons that appear to be required for the phenomenological success of liquid instanton models [3].

For full QCD the range of our calculations has been necessarily limited and further work is needed. We have performed exploratory calculations of some flavour-singlet meson masses

and appear to obtain an  $\eta'$  mass that remains massive in the chiral limit, and is  $\sim 1\text{GeV}$  if we introduce ‘physical units’ in the simplest possible fashion. Mass calculations using the eigenvectors of the Dirac operator would be of particular interest, not least because they would allow us to test for the presence of a massless Goldstone pion. Moreover, the fact that the eigenvectors become much more extended in space-time as  $\lambda \rightarrow 0$  (as we saw in quenched QCD) should have phenomenological consequences.

While we now feel that we have convincing evidence for the claim that the mixing of would-be instanton zero-modes will generically produce chiral symmetry breaking and a  $\lambda \rightarrow 0$  divergence in the Dirac spectral density, we cannot of course be sure that this survives in the full field theory. For example, if there is some other dynamical mechanism that produces a non-zero density of modes at  $\lambda = 0$ , then the latter will mix with the (mixed) would-be zero-modes near  $\lambda = 0$ , and we cannot be certain that the divergence in the latter will survive. Equally, if it should be that the modes in the divergent peak have a space-time extent that  $\rightarrow \infty$  as  $\lambda \rightarrow 0$ , then they might well be suppressed by the confining fluctuations of the theory. There are obvious ways that we can, and should, investigate these possibilities within our model.

An intriguing question is whether there is any relation between the divergence that we have found and the logarithmic divergence that appears in quenched chiral perturbation theory [16]. A link is plausible because the strength of the chiral logarithm is determined by the strength,  $\delta$ , of the pseudoscalar flavour singlet annihilation diagram which itself is determined by the topological fluctuations of the quenched vacuum (and whose iteration, in full QCD, produces the  $\eta'$  mass). If  $\delta$  is indeed small at the large instanton densities where our divergence becomes weak enough to be fit with a logarithm [10], then the consistency of the two approaches becomes possible. Indeed one can argue [18] that the chiral logarithm will become a power if one sums leading logs to all orders in chiral perturbation theory. Of course once  $\delta$  becomes large these perturbative calculations might become unreliable. In that case our model may provide a non-perturbative method for calculating the fate of these quenched chiral logarithms. Of course, one might ask how the power divergence that we see



in full QCD fits into all this. We conjecture that it might be related, in a fashion analogous to the above, to the remnant chiral logarithms in partially quenched QCD. This scenario can and should be tested within our model.

## VII. ACKNOWLEDGEMENTS

MT wishes to acknowledge Nigel Dowrick's important influence on this work, through their extensive, but largely unpublished, collaboration some seven years ago. We wish to thank PPARC for support under grant GR/K55752. US also wishes to thank PPARC for a research studentship (number 96314624). The computations were performed on our Departmental workstations.

## REFERENCES

- [1] D.G. Caldi, Phys. Rev. Lett. **39** (1977) 121.  
C.G. Callan, R. Dashen and D.J. Gross, Phys. Rev. **D17** (1978) 2717.  
R.D. Carlitz and D.B. Creamer, Ann. Phys. **118** (1979) 429.
- [2] D. Diakonov, hep-ph/9602375.
- [3] T. Schafer and E.V. Shuryak, Rev. Mod. Phys. **70** (1998) 323
- [4] T. Banks and A. Casher, Nucl. Phys. **B169** (1980) 103.
- [5] M.F. Atiyah and I.M. Singer, Annals Math. **87** (1968) 484.  
M.F. Atiyah and I.M. Singer, Annals Math. **87** (1968) 546.
- [6] C.E. Carneiro and N.A. McDougall, Nucl. Phys. **B245** (1984) 293.
- [7] N. Dowrick and M. Teper, Nucl. Phys. Proc. Suppl. **42** (1995) 237.
- [8] D.A. Smith and M.J. Teper [UKQCD Collaboration], Phys. Rev. **D58** (1998) 014505
- [9] M. Garcia Perez, O. Philipsen and I-O Stamatescu, Nucl.Phys. B551 (1999) 293.  
A. Hasenfratz and C. Nieter, Phys. Lett. B439 (1998) 366.  
T. DeGrand, A. Hasenfratz and T. Kovacs, Nucl. Phys. B520 (1998) 301.  
Ph. de Forcrand, M. Garcia Perez and I-O Stamatescu, Nucl. Phys. B499 (1997) 409.  
R. Brower et al, Nucl. Phys. Proc. Suppl. 53 (1997) 547.
- [10] U. Sharan and M. Teper [UKQCD Collaboration], Phys. Rev. **D60** (1999) 054501
- [11] J. Negele, hep-lat/9810053; hep-lat/9902032.
- [12] N. Dowrick and M. Teper, unpublished.
- [13] J. Verbaarschot, hep-th/9710114.  
J.J. Verbaarschot, hep-lat/9908002.
- [14] U. Sharan and M. Teper, Nucl. Phys. Proc. Suppl. **73** (1999) 617

- [15] E.V. Shuryak and J.J. Verbaarschot, Phys. Rev. Lett. **68** (1992) 2576.
- [16] S.R. Sharpe, Nucl. Phys. Proc. Suppl. **17** (1990) 146.  
C. Bernard and M. Golterman, Nucl. Phys. Proc. Suppl. **26** (1992) 360.  
M. Golterman, hep-ph/9710468.
- [17] J.C. Osborn and J.J. Verbaarschot, Nucl. Phys. **B525** (1998) 738  
J.C. Osborn, D. Toublan and J.J. Verbaarschot, Nucl. Phys. **B540** (1999) 317  
J. Verbaarschot, private communication.  
E. Shuryak, private communication.
- [18] S.R. Sharpe, Nucl. Phys. Proc. Suppl. **30** (1993) 213  
M. Golterman, private communication.
- [19] J.B. Kogut, J.F. Lagae and D.K. Sinclair, Phys. Rev. **D58** (1998) 054504
- [20] T. Banks and A. Zaks, Nucl. Phys. B196 (1982) 173.  
Y. Iwasaki et al, hep-lat/9804005.
- [21] J. Kogut, D. Sinclair and M. Teper, Phys. Rev. D44 (1991) 2869.

TABLES

Type	$f$	$V$	$N_c$	d	$\chi_p^2/N_{DF}$	$\chi_l^2/N_{DF}$
Hard Sphere	0.2	1.0	650000	0.656±0.003	2.40	600
	0.5	1.0	128000	0.695±0.002	1.92	508
	1.0	0.41	130000	0.540±0.003	1.71	123
	1.0	1.0	126000	0.595±0.002	1.38	258
	1.0	1.52	97000	0.617±0.001	1.23	400
	1.0	2.44	93000	0.640±0.001	1.47	702
	1.0	7.72	9780	0.668±0.003	1.73	456
	1.75	1.0	111000	0.309±0.002	1.94	48
	2.5	1.0	63200	0.075±0.014	1.72	2.59
	5.3	1.0	6720	0.004±0.010	2.20	2.19
Gaussian	10.0	1.0	1266	0.008±0.016	1.91	1.90
	1.0	1.0	12600	0.588±0.005	1.36	45
	1.0	2.4	15500	0.634±0.002	1.31	201
	2.5	1.0	6320	0.290±0.007	1.46	4.87
Classical	1.0	1.0	2100	0.477±0.010	1.32	5.33
	1.0	2.4	450	0.538±0.022	1.38	3.50
Class. (II)	1.0	1.0	2520	0.555±0.006	1.56	34.6

TABLE I. Parameters and results for  $Q = 0$ ,  $N_f = 0$  ensembles.  $f$  is the packing fraction,  $V$  is the space-time volume,  $N_c$  is the number of configurations in the ensemble,  $d$  is the degree of divergence,  $\chi_p^2/N_{DF}$  is the chi-square for the best power fit to the divergence and  $\chi_l^2/N_{DF}$  is the chi-square for the best log fit.

Type	$f$	$V$	$N_c$	d	$\chi_p^2/N_{DF}$	$\chi_l^2/N_{DF}$
Hard Sphere	1.0	1.0	126000	$0.363 \pm 0.006$	1.90	65
	1.0	2.4	62000	$0.522 \pm 0.003$	2.07	253

TABLE II. Parameters and results for  $N_f = 0$  ensembles with variable  $Q$  and  $N$ .  $f$  is now the mean packing fraction.

Type	$f$	$V$	$\delta\rho(0, 2)$	$\delta\rho(2, 4)$	$\delta\rho(4, 6)$
Hard Sphere	0.77	0.41	0.88(3)	0.75(4)	0.68(3)
	2.96	0.11	0.85(3)	0.75(3)	0.67(3)

TABLE III. Values of  $\delta\rho(|Q|, |Q| + 2)$ , as defined in the text, for two different  $N_f = 0$  hard sphere ensembles.

Set	$\bar{\lambda}_{NZ}$	$N_f$	$m$	$\langle Q^2 \rangle$	$\langle N_I \rangle$
A	2.0	1	0.5	$25.65 \pm 0.45$	35.53
B	2.0	1	0.3	$14.28 \pm 0.16$	34.91
C	2.0	1	0.15	$8.13 \pm 0.04$	35.75
D	2.0	2	0.5	$5.04 \pm 0.04$	21.35
E	2.0	2	0.3	$2.43 \pm 0.03$	23.17
F	2.0	2	0.15	$0.72 \pm 0.01$	30.85
G	-	1	3.0	$98.615 \pm 0.78$	62.80
H	-	1	2.0	$80.097 \pm 0.92$	63.03
I	-	1	1.0	$60.383 \pm 0.49$	62.95
J	-	1	0.5	$34.22 \pm 0.26$	62.98
K	-	1	0.3	$22.00 \pm 0.19$	62.99
L	-	1	0.15	$11.66 \pm 0.07$	63.01
M	-	2	3.0	$83.20 \pm 0.64$	63.07
N	-	2	2.0	$62.49 \pm 0.40$	62.90
O	-	2	1.0	$31.37 \pm 0.13$	62.93
P	-	2	0.5	$11.61 \pm 0.10$	62.98
Q	-	2	0.3	$4.71 \pm 0.05$	62.96
R	-	2	0.15	$0.89 \pm 0.02$	62.98

TABLE IV. Some information about the  $N_f \neq 0$  full QCD ensembles. Where  $N$  has been kept fixed, a value for  $\bar{\lambda}_{NZ}$  is not needed, and is not given.

Set	b	d	$\chi^2/N_{DF}$	$m_{\eta'}$	$m_{\sigma}$
A	2.904±0.158	0.668±0.008	1.09	11.2±2.0	11.3±2.5
B	1.956±0.181	0.699±0.017	0.94	12.9±2.5	10.9±1.8
C	0.491±0.058	0.861±0.022	2.41	11.5±1.5	10.2±2.4
D	0.228±0.031	0.882±0.021	1.15	17.3±1.9	15.2±2.0
E	0.043±0.009	0.979±0.032	1.44	19.3±2.0	17.4±2.7
F	-	-	-	20.0±2.0	16.7±2.2
G	30.917±3.324	0.300±0.018	0.99	8.9±3.1	-
H	28.766±2.058	0.307±0.013	1.35	8.5±2.5	-
I	36.517±4.636	0.252±0.019	1.41	11.5±2.2	-
J	24.048±2.936	0.288±0.019	2.05	11.7±2.1	-
K	17.599±2.632	0.309±0.023	3.27	12.4±2.9	-
L	4.395±0.586	0.478±0.024	4.20	12.1±2.3	-
M	30.410±3.919	0.296±0.020	1.17	9.5±3.7	-
N	30.990±2.520	0.285±0.014	1.57	13.6±2.7	-
O	17.665±1.714	0.343±0.017	1.41	15.0±3.6	-
P	4.404±0.267	0.519±0.013	1.99	20.6±2.5	-
Q	0.580±0.051	0.788±0.019	1.55	15.8±2.5	-
R	0.006±0.002	1.307±0.043	2.30	18.2±2.1	-

TABLE V. Parameters of power-law fits to the spectral densities, for the ensembles given in table IV, as well as mass estimates for the  $\eta'$  and  $\sigma$  mesons.

## FIGURES

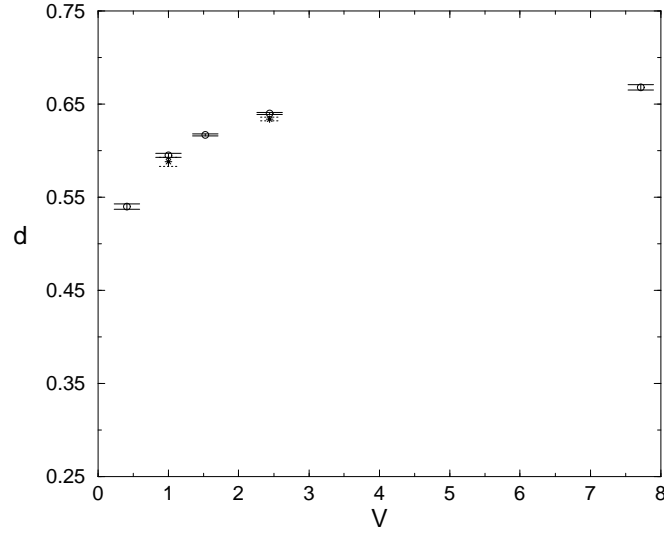


FIG. 1. Exponent of power divergence,  $d$ , versus space-time volume  $V$ . Hard sphere ( $\circ$ ) and Gaussian ( $\star$ ) wavefunctions, with density  $f = 1$ .

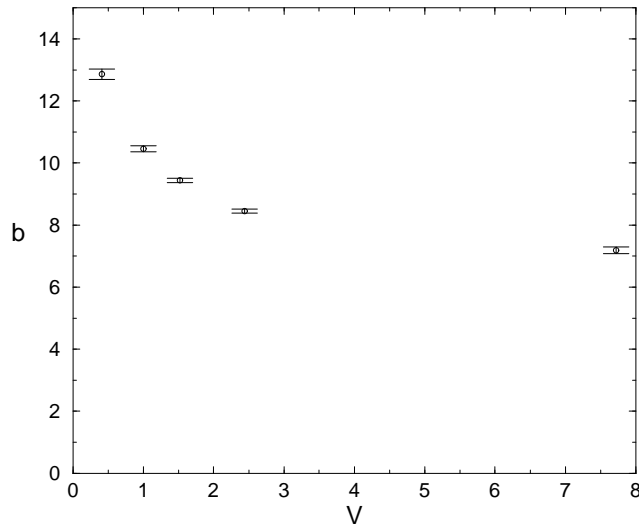


FIG. 2. Volume dependence of the coefficient  $b$  of the  $1/\lambda^d$  piece in the spectral density. For hard spheres as in figure 1.



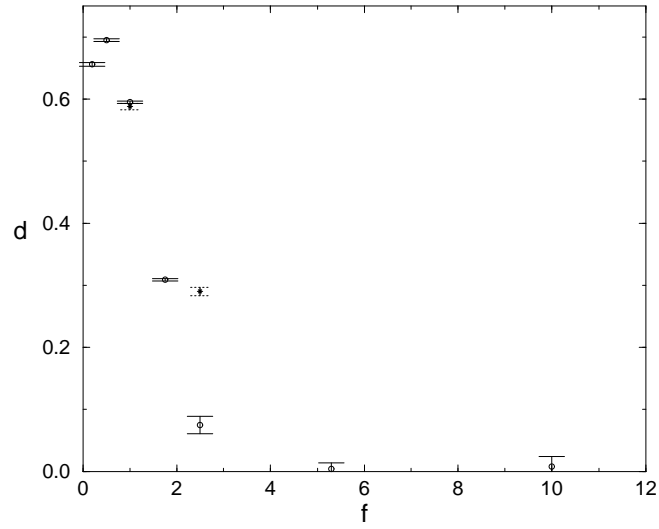


FIG. 3. Exponent of power divergence,  $d$ , versus packing fraction  $f$ . Hard sphere ( $\circ$ ) and Gaussian ( $\star$ ) wavefunctions, with volume  $V = 1$ .

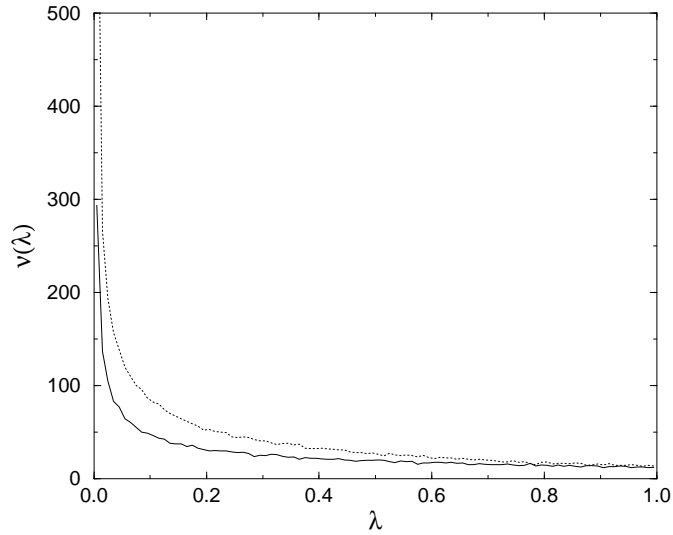


FIG. 4. Spectral density using classical zero mode wavefunctions. Our usual approximation to  $i\mathcal{D}[A]$  (solid) compared to that using the linear addition ansatz (dotted).

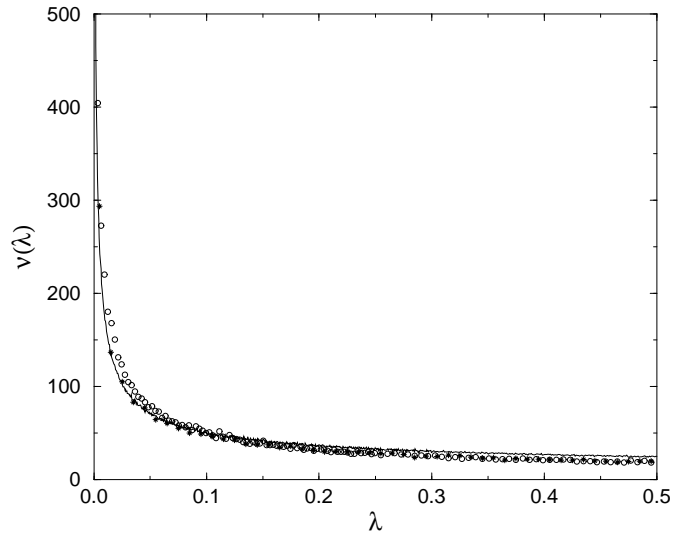


FIG. 5. The spectral densities obtained at  $f = 1$ ,  $V = 1$  from hard sphere (solid), Gaussian ( $\circ$ ) and classical zero mode ( $\star$ ) wavefunctions.

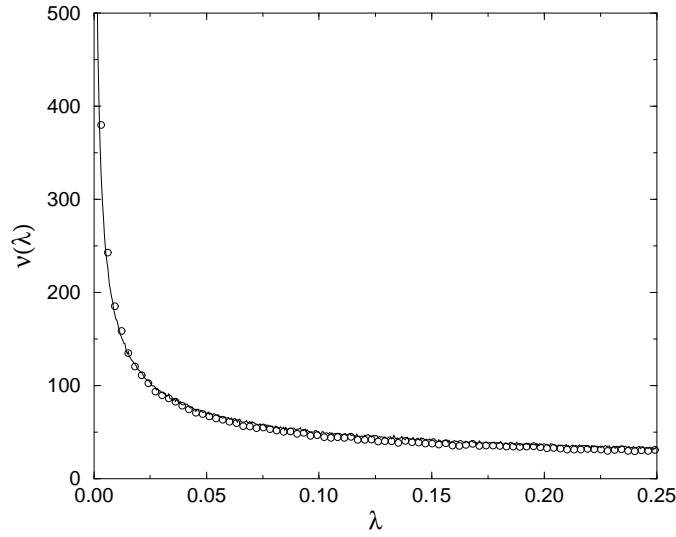


FIG. 6. Comparing spectral densities on  $\mathbb{R}^4$  ( $\circ$ ) and on  $\mathbb{T}^4$  (solid), with hard sphere wavefunctions for  $f = 1$ ,  $V = 1$ .

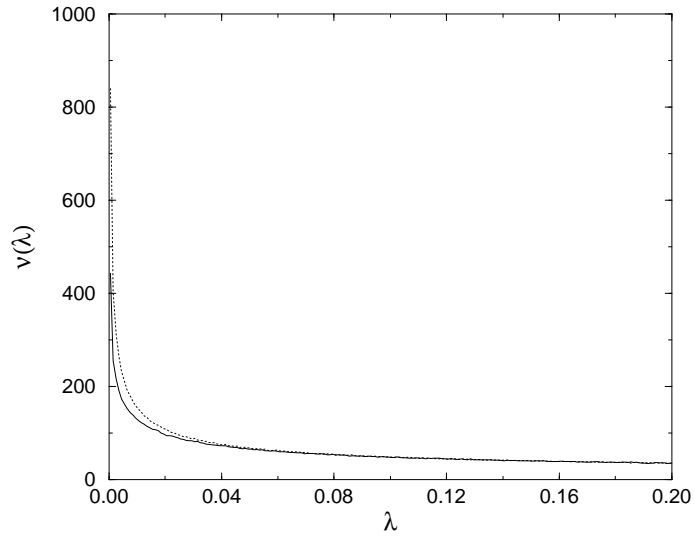


FIG. 7. Spectral densities with variable  $Q$  on two volumes:  $V = 1$  (solid) and  $V \approx 2.44$  (dashed). With hard spheres and  $f = 1$ .

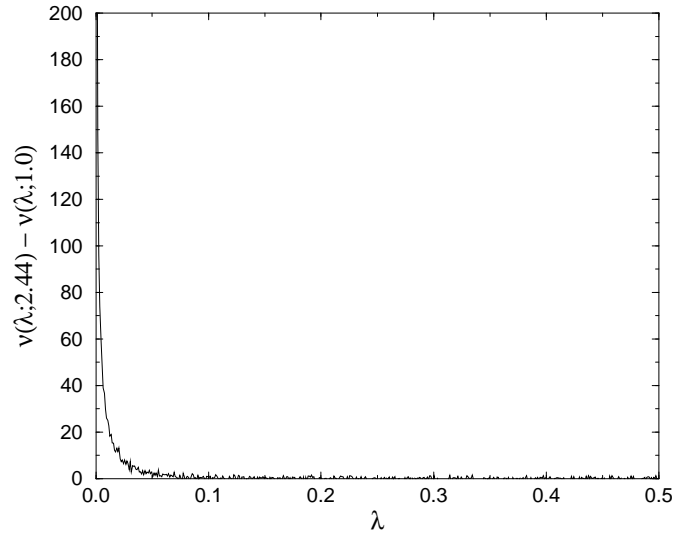


FIG. 8. The difference of the two spectral densities in figure 7.

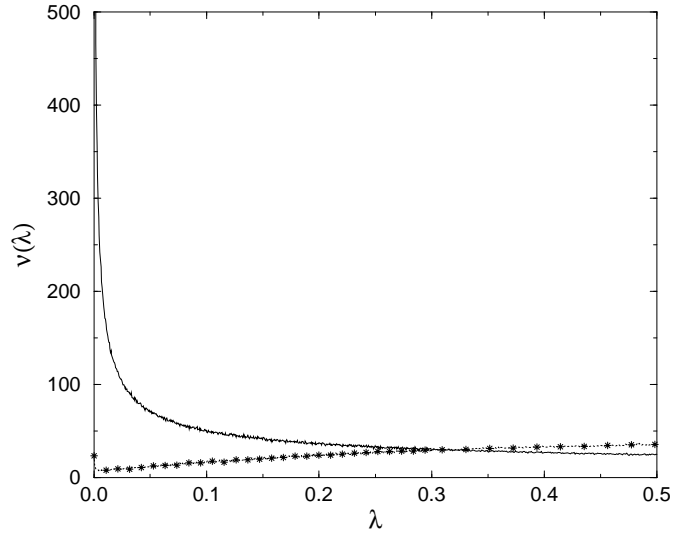


FIG. 9. Actual spectral density (solid) compared to background curve ( $\star$ ) from pairwise eigenvalue splitting as defined in the text. Hard spheres with  $V = 1$ ,  $f = 1$ .

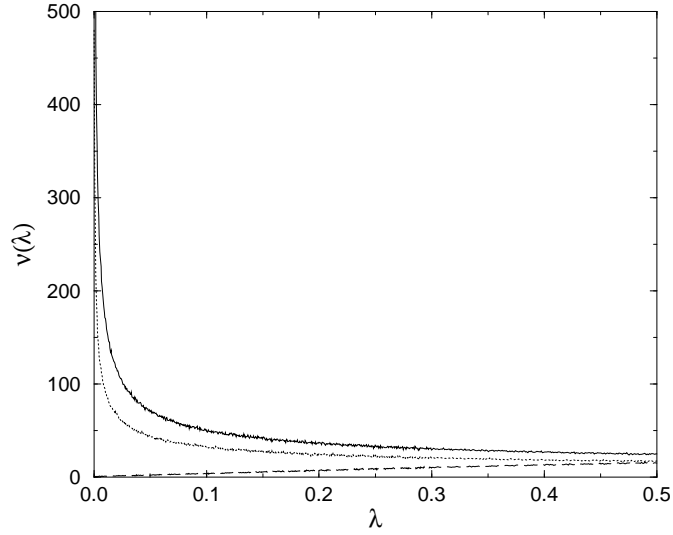


FIG. 10. Spectral densities: instanton gas (solid), dipole gas with maximum separation  $|x^+ - x^-| \leq 2\rho$  (dotted); background curve for dipole gas (long dashed). Using hard spheres and  $V = 1$ ,  $f = 1$ .

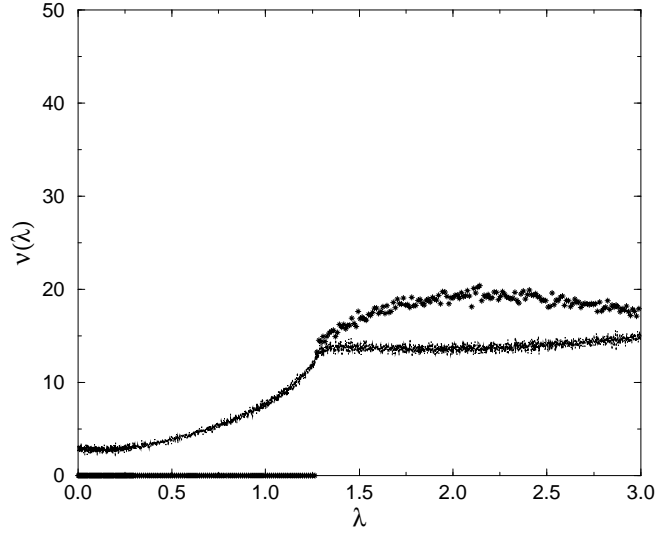


FIG. 11. Actual spectral density (dotted) compared to background curve ( $\star$ ) for a dipole gas with maximum separation  $|x^+ - x^-| \leq 2\rho$ . With  $V = 1$ ,  $f = 1$ .

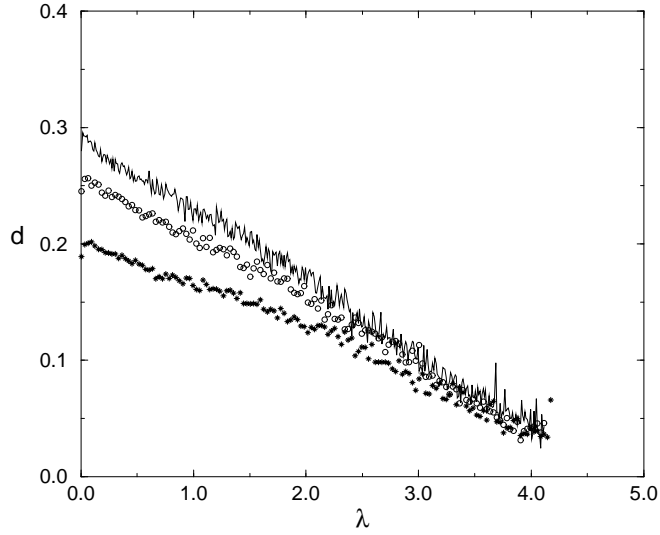


FIG. 12. Size of eigenfunctions of  $i\mathcal{D}$  versus  $\lambda$ . For volumes  $V = 0.4096$  ( $\star$ ),  $V = 1$  ( $\circ$ ) and  $V \approx 1.5$  (solid) using  $f = 1$  hard spheres.

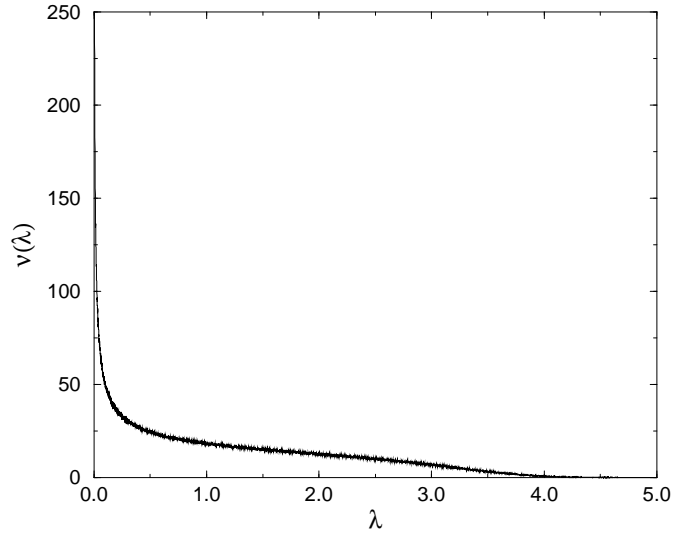


FIG. 13. The spectral density for  $f = 1$ ,  $V = 1$ ,  $N_f = 0$  plotted for the full range of  $\lambda$ .

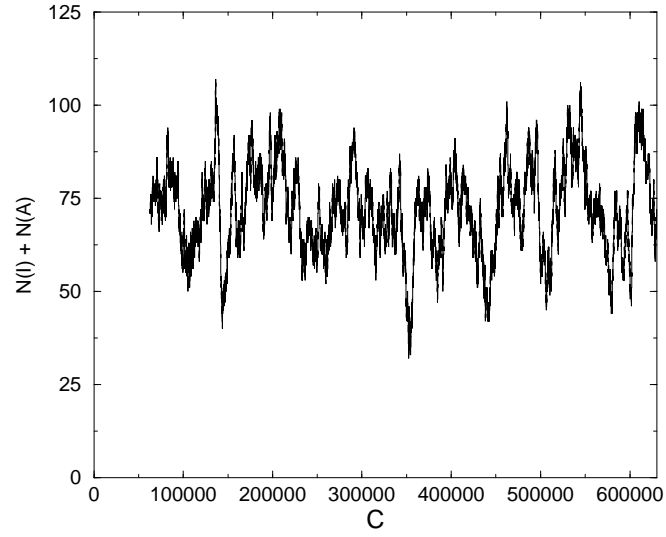


FIG. 14.  $N_f = 1$ ,  $\bar{\lambda}_{NZ} = 2.0$ ,  $V = 1$ ,  $m = 0.15$ . The total number of objects as a function of the configuration number in the Monte Carlo sequence.

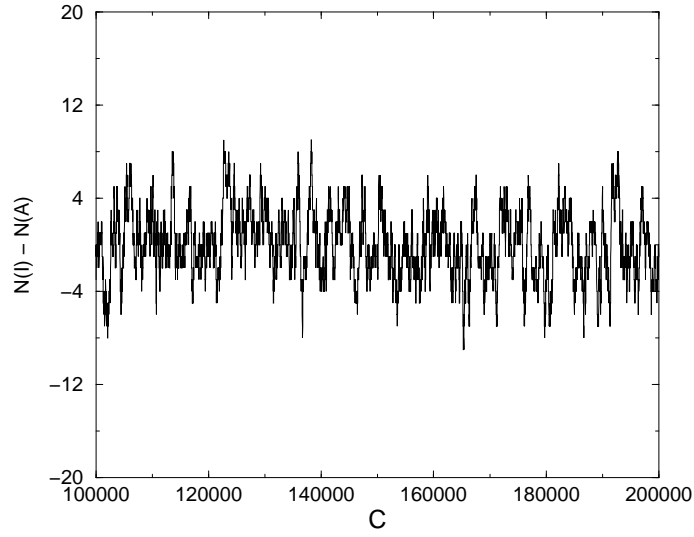


FIG. 15.  $N_f = 1$ ,  $\bar{\lambda}_{NZ} = 2.0$ ,  $V = 1$ ,  $m = 0.15$ . The net winding number as a function of the configuration number. We show only a section of the run for clarity.

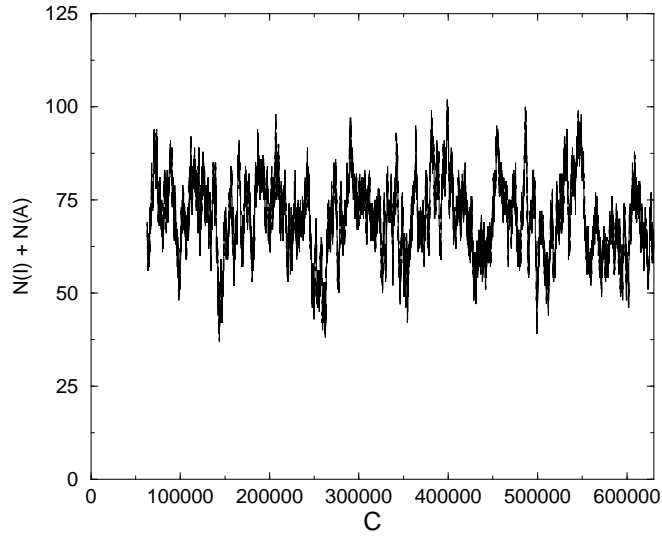


FIG. 16.  $N_f = 1$ ,  $\bar{\lambda}_{NZ} = 2.0$ ,  $V = 1$ ,  $m = 0.5$ . The total number of objects as a function of the configuration number.

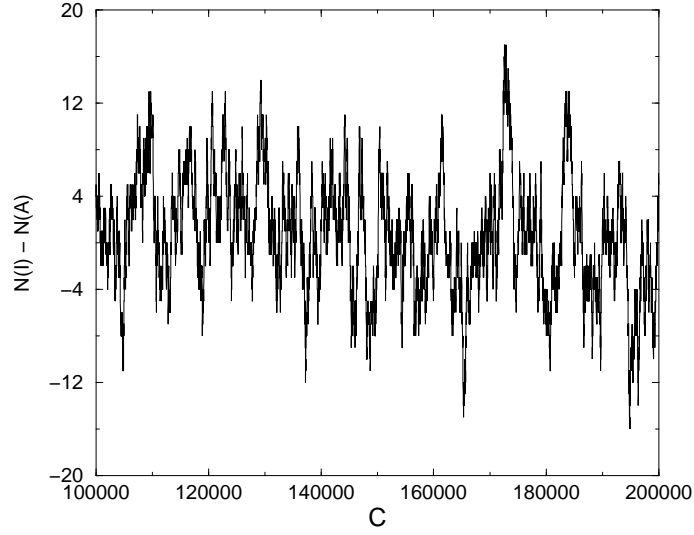


FIG. 17.  $N_f = 1$ ,  $\bar{\lambda}_{NZ} = 2.0$ ,  $V = 1$ ,  $m = 0.5$ . The net winding number as a function of the configuration number. We show only a section of the run for clarity.

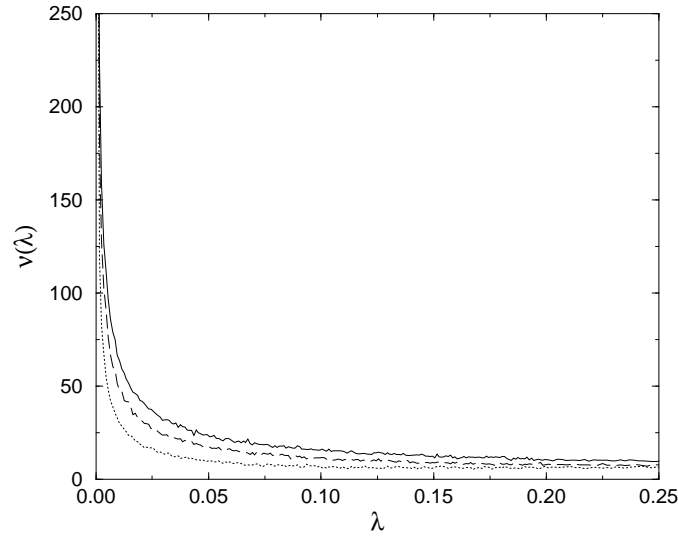


FIG. 18.  $N_f = 1$ ,  $\bar{\lambda}_{NZ} = 2.0$ ,  $V = 1$ . The spectral density for quark mass  $m = 0.5$  (solid),  $0.3$  (long dashed) and  $0.15$  (dotted).



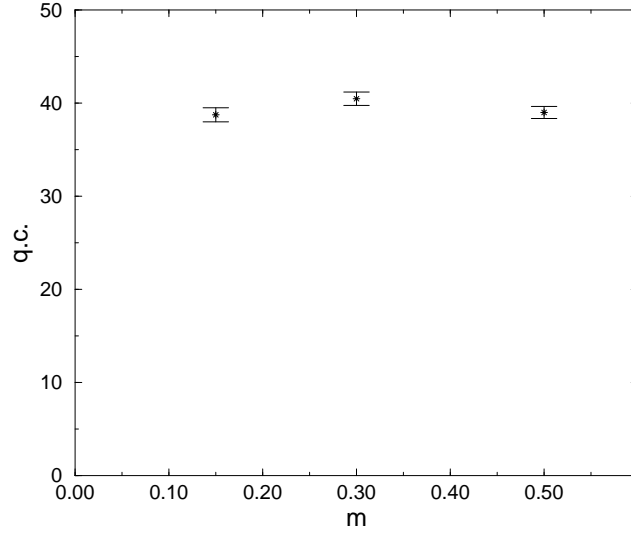


FIG. 19. The quark condensate  $\langle \bar{\psi}\psi \rangle$  as a function of the quark mass  $m$  from the spectra plotted in figure 18.

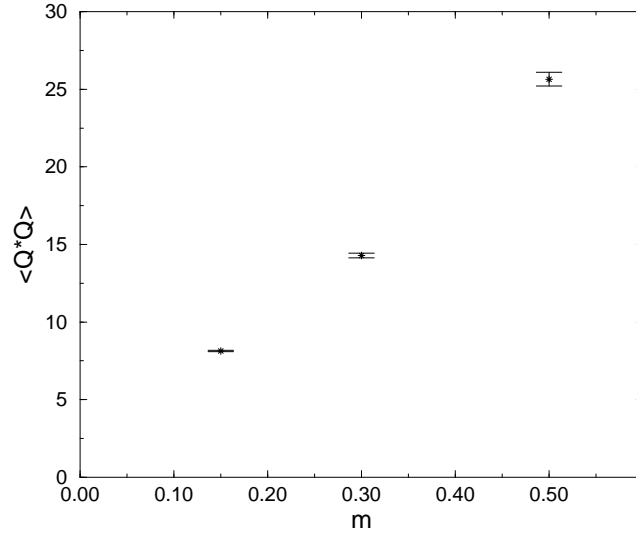


FIG. 20.  $N_f = 1$ ,  $\bar{\lambda}_{NZ} = 2.0$ ,  $V = 1$ . The second moment of the winding number distribution  $\langle Q^2 \rangle$  as a function of the quark mass  $m$ .

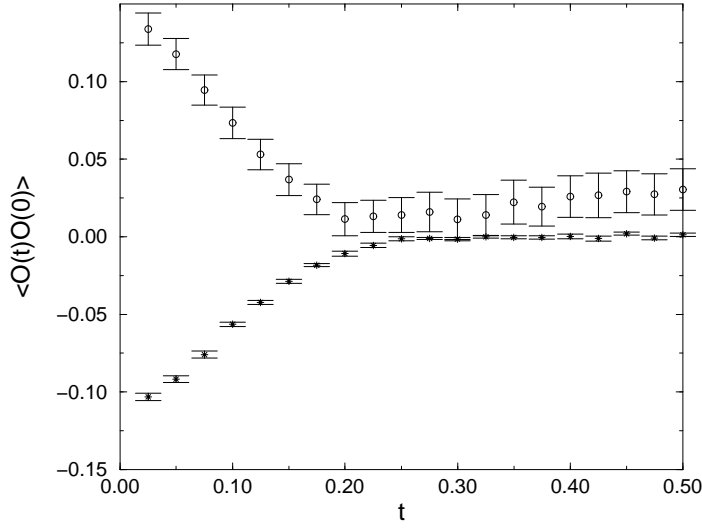


FIG. 21.  $N_f = 1$ ,  $\bar{\lambda}_{NZ} = 2.0$ ,  $V = 1$ ,  $m = 0.15$ . Correlation functions for  $\eta'$  ( $\star$ ), and for  $\sigma$  ( $\circ$ ).

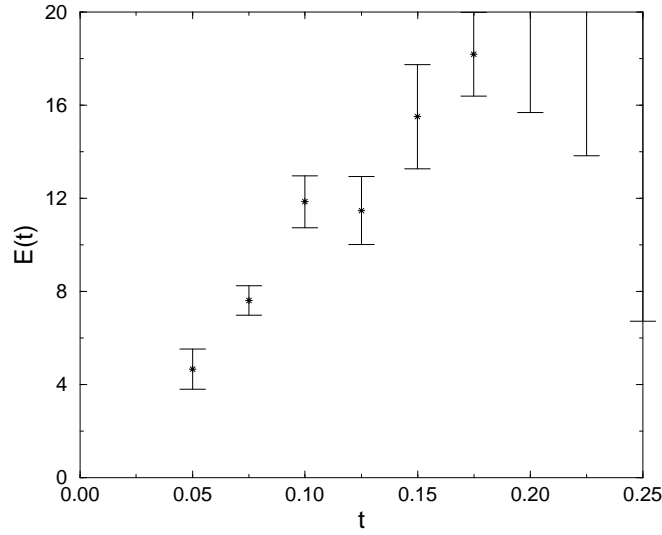


FIG. 22.  $N_f = 1$ ,  $\bar{\lambda}_{NZ} = 2.0$ ,  $V = 1$ ,  $m = 0.15$ . The  $\eta'$  effective mass from the correlation functions shown in figure 21.

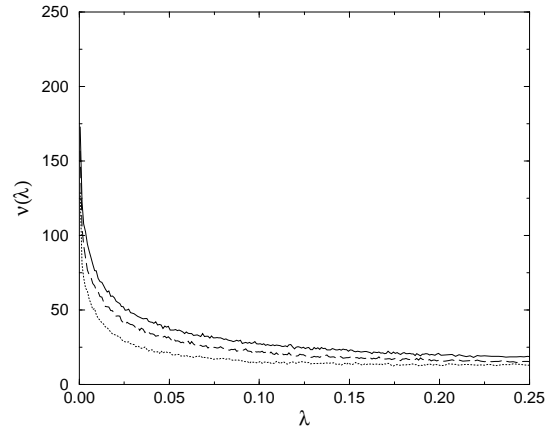


FIG. 23.  $N_f = 1$ , Fixed  $N$ ,  $V = 1$ . The spectral density for quark mass  $m = 0.5$  (solid),  $0.3$  (long dashed) and  $0.15$  (dotted).

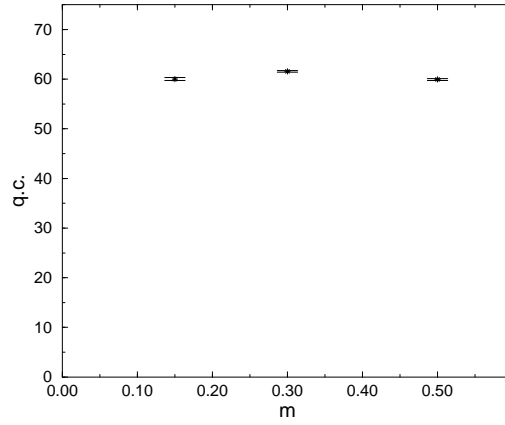


FIG. 24.  $N_f = 1$ , Fixed  $N$ ,  $V = 1$ . The quark condensate  $\langle \bar{\psi}\psi \rangle$  as a function of the quark mass  $m$ .

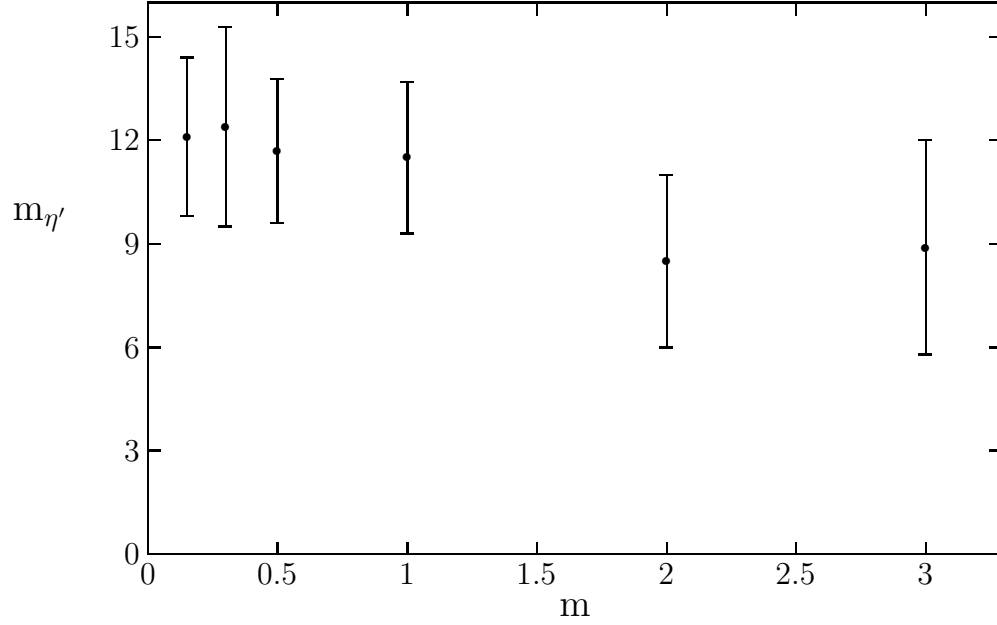


FIG. 25.  $N_f = 1$ ,  $V = 1$ . The mass of the  $\eta'$  as a function of the quark mass.

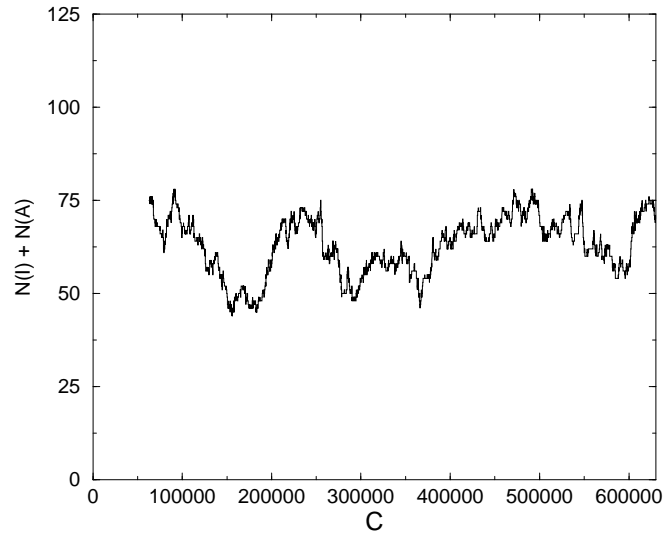


FIG. 26.  $N_f = 2$ ,  $\bar{\lambda}_{NZ} = 2.0$ ,  $V = 1$ ,  $m = 0.15$ . The total number of objects as a function of the configuration number.

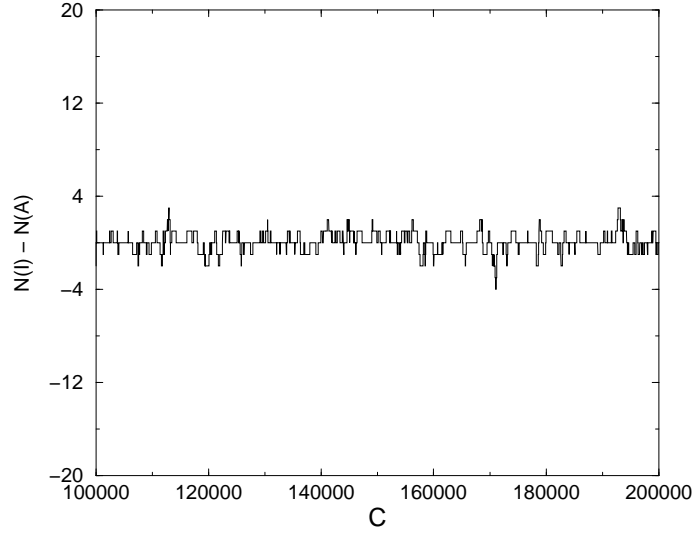


FIG. 27.  $N_f = 2$ ,  $\bar{\lambda}_{NZ} = 2.0$ ,  $V = 1$ ,  $m = 0.15$ . The net winding number as a function of the configuration number. We show only a section of the run for clarity.

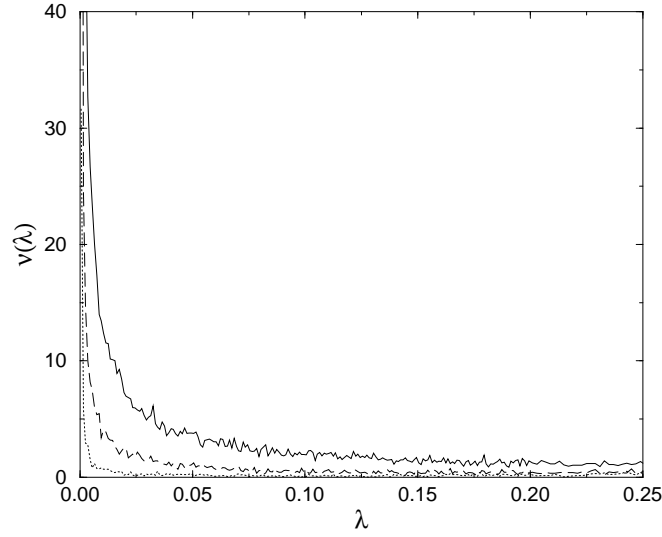


FIG. 28.  $N_f = 2$ ,  $\bar{\lambda}_{NZ} = 2.0$ ,  $V = 1$ . The spectral density for quark mass  $m = 0.5$  (solid),  $0.3$  (long dashed) and  $0.15$  (dotted).

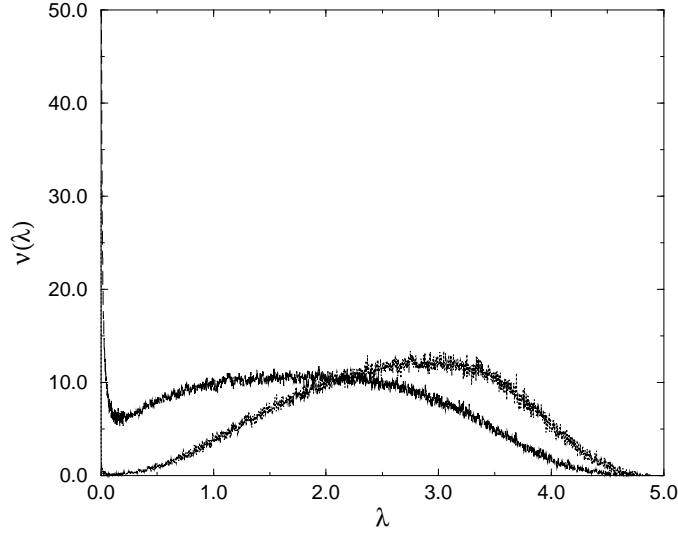


FIG. 29.  $\bar{\lambda}_{NZ} = 2.0$ ,  $V = 1$ ,  $m = 0.15$ . A comparison of the spectral densities obtained for  $N_f = 1$  (dark-solid) and  $N_f = 2$  (light-dotted).

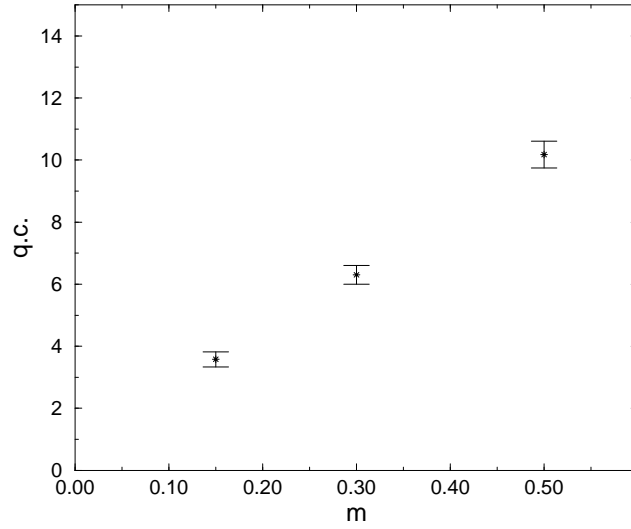


FIG. 30. The quark condensate  $\langle \bar{\psi}\psi \rangle$  as a function of the quark mass  $m$  from the  $N_f = 2$  spectra plotted in figure 28.

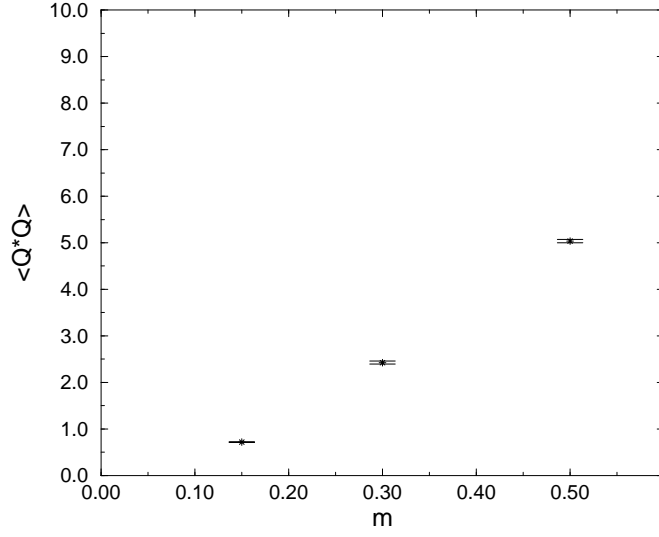


FIG. 31.  $N_f = 2$ ,  $\bar{\lambda}_{NZ} = 2.0$ ,  $V = 1$ . The second moment of the winding number distribution  $\langle Q^2 \rangle$  as a function of the quark mass  $m$ .

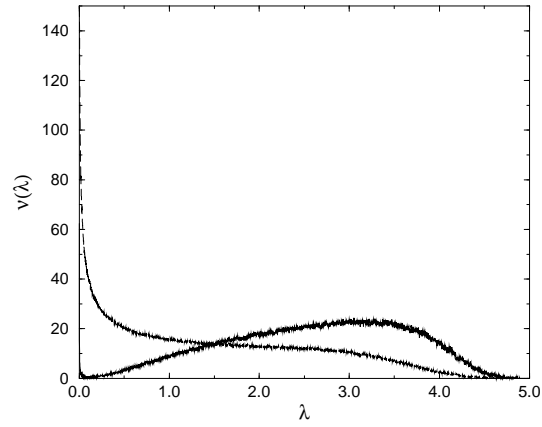


FIG. 32.  $N_f = 2$ , Fixed  $N$ ,  $V = 1$ . The spectral density for quark mass  $m = 0.15$  (solid) and  $m = 3.0$  (long dashed).

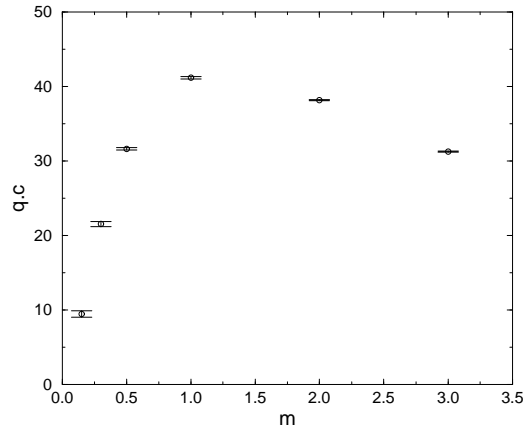


FIG. 33.  $N_f = 2$ , Fixed  $N$ ,  $V = 1$ . The quark condensate  $\langle \bar{\psi}\psi \rangle$  as a function of the quark mass  $m$ .

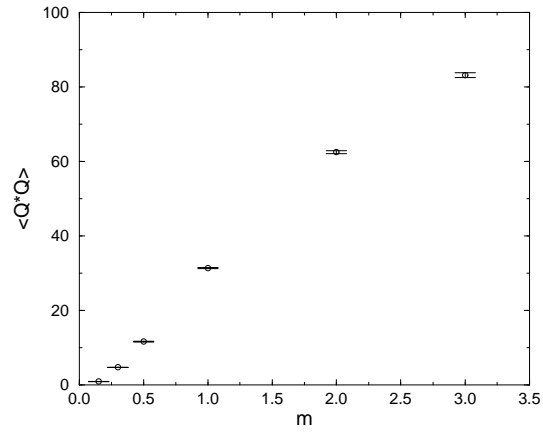


FIG. 34.  $N_f = 2$ , Fixed  $N$ ,  $V = 1$ . The second moment of the winding number distribution  $\langle Q^2 \rangle$  as a function of the quark mass  $m$ .